TU Delft

Delft University of Technology

Document Version
Final published version

Licence
Dutch Copyright Act (Article 25fa)

Citation (APA)
Persoons, R., & van Mieghem, P. (2026). Susceptible-infectious-susceptible epidemics on temporal contact graphs with clique structure. *Physical Review E*, *114*(4), Article 044304. https://doi.org/10.1103/6jqp-bz2r

Important note
To cite this publication, please use the final published version (if applicable).
Please check the document version above.

Copyright
In case the licence states “Dutch Copyright Act (Article 25fa)”, this publication was made available Green Open Access via the TU Delft Institutional Repository pursuant to Dutch Copyright Act (Article 25fa, the Taverne amendment). This provision does not affect copyright ownership.
Unless copyright is transferred by contract or statute, it remains with the copyright holder.

Sharing and reuse
Other than for strictly personal use, it is not permitted to download, forward or distribute the text or part of it, without the consent of the author(s) and/or copyright holder(s), unless the work is under an open content license such as Creative Commons.

Takedown policy
Please contact us and provide details if you believe this document breaches copyrights.
We will remove access to the work immediately and investigate your claim.

This work is downloaded from Delft University of Technology.

Susceptible-infectious-susceptible epidemics on temporal contact graphs with clique structure

Robin Persoons* and Piet Van Mieghem
Faculty of Electrical Engineering, Mathematics, and Computer Science, Delft University of Technology, P.O. Box 5031, 2600 GA Delft, The Netherlands

(Received 21 November 2025; revised 21 July 2026; accepted 9 September 2026; published 2 October 2026)

We consider temporal networks that are a union of disjoint cliques at all times t. We call temporal networks that consist of disjoint cliques *temporal clique graphs*. We extend the exact solution of mean-field SIS epidemics with self-infections on the complete graph, derived by Prasse *et al.* [Chaos **31**, 063115 (2021)], to all temporal clique graphs. Temporal clique graphs cover a range of commonplace models of network dynamics, including metapopulation models and specifically random-walker-induced temporal graphs. Since the exact solution of mean-field SIS on temporal clique graphs is piecewise (i.e., given by different functions on different intervals), we apply further approximations and find an approximate expression for the expected fraction of infected individuals, called the prevalence $y(t)$, at all times t, with as parameters only the infection rate β, the curing rate δ, and the average size θ_j of each clique j in the steady state of the network dynamics. Our strongest assumption is that the contact network is static and in its steady state, effectively ignoring all graph dynamics. Despite the drastic assumptions, in ignoring any temporal aspects of the contact network, the approximation is remarkably accurate, when the number of walkers is high. We assess our prevalence approximation (15) and indicate and explain its accuracy.

DOI: 10.1103/6jqp-bz2r

I. INTRODUCTION

Metapopulation models [1,2] have been widely used in network epidemiology [3–5]. Metapopulation models are characterized by their clique structure: all individuals are divided among subpopulations and interact only with those individuals that are in the same subpopulation or clique. Individuals generally move between subpopulations according to a global rule that is the same for each individual. Within each subpopulation, individuals generally interact with each other under the assumption of homogeneous mixing. *Homogeneous mixing* dictates that each individual is equally likely to interact with any another individual and is thus equally likely to infect or be infected by any other individual. While homogeneous mixing does not describe reality, because an individual is more likely to infect/to be infected by those that are nearby, homogeneous mixing models have been a cornerstone of epidemiology since the first compartmental model by Kermack and McKendrick [6].

Almasan *et al.* [7] describe the random-walker-induced temporal contact graphs (RWIG) model, which is an extension of the metapopulation model. In RWIG, M random walkers move between the N nodes of the node set $\mathcal{N}$ according to (different) walker policies. If two walkers n and m are in the same node $i \in \mathcal{N}$ at time t, they are in contact with each other at time t. The RWIG model is extended to continuous-time in Ref. [8]. Temporal networks generated by RWIG have a clique structure at all times due to the colocation principle: walkers form cliques with each other in each node of the node set $\mathcal{N}$. The nodes of the node set $\mathcal{N}$ are equivalent to the subpopulations in the metapopulation model. However, instead of a global rule that describes the movements of individuals, each individual has its own mobility pattern described by its own *policy*, specified by a general Markov transition probability matrix or infinitesimal generator. It is demonstrated in Ref. [7] that the clique structure obtained from the colocation assumption is in agreement with real-world data from Ref. [9].

Exact analytical results in epidemics on temporal networks are remarkably rare. The epidemic threshold in temporal networks for *discrete-time* SIS is derived in Ref. [10] and again in Ref. [11], while extended to *continuous-time* for weakly commuting networks in Ref. [12]. Exact results also appear for specific temporal network models, such as activity driven networks [13], rewired configuration models [14] and time-variant trees [15].

Analytic results for epidemics on temporal networks often assume *timescale separation*. When the temporal network changes significantly faster than the epidemic spreads, the network is called *annealed*. In the annealed regime, the virus "sees" only the average of each link and thus the network can be accurately approximated by its link-time-average [12,16,17]. When the network changes significantly slower than the epidemic process, the network is called *quenched*. In the quenched regime, the virus does not "see" the network changing at all. The network can, therefore, be approximated as static. Between the annealed and quenched regime lies the

*Contact author: r.d.l.persoons@tudelft.nl

Published by the American Physical Society under the terms of the Creative Commons Attribution 4.0 International license. Further distribution of this work must maintain attribution to the author(s) and the published article's title, journal citation, and DOI.

intermediate regime, where neither of the above approximations is accurate, because the network and virus change on the same timescale.

In this work, we present three results on temporal clique graphs. First, we extend the exact solution of the SIS N-intertwined mean-field approximation (NIMFA) with self-infections from Ref. [18] to any temporal clique graph. Because NIMFA on a temporal network is defined piecewise, i.e., with different governing equations on different intervals [19], the exact solution will also be in a piecewise form.

Second, we use the observation that the steady-state prevalence, or fraction of infected walkers, changes with the speed of the network dynamics to define the *lower transition time* $\underline{\mathrm{T}}(r)$ for NIMFA on RWIG. In Ref. [19], the upper-transition time $\overline{\mathrm{T}}(r)$ and the lower- transition time $\underline{\mathrm{T}}(r)$ are introduced as the boundaries of the intermediate regime. The lower transition time $\underline{\mathrm{T}}(r)$ was only introduced as a concept in Ref. [19], and could not be defined formally due to this missing insight about the steady-state prevalence.

Our third result is a closed-form approximate formula of the SIS prevalence on RWIG. We derive our closed form after a series of approximations: (i) we approximate the Markovian stochastic SIS process with the NIMFA mean-field approximation; (ii) we allow for self-infections; (iii) we assume the RWIG process is in steady state; (iv) we assume there are no walker movements; and (v) we assume that all walkers in each location have the same infection probability at all times t. After our approximations, we find a closed form that is a function of only the infection parameters β and δ, the number of walkers M, the size of the RWIG node-set $|\mathcal{N}| = N$ and the expected steady-state clique sizes $\theta_1, \ldots, \theta_N$. Our prevalence approximation is independent of the realization of the temporal contact graph. Despite these rather strong assumptions, the accuracy of the prevalence approximation under different circumstances is surprisingly good. Within our approximations, we sketch how an analytical approximation of the lower transition time $\underline{\mathrm{T}}(r)$ can be computed.

This paper is structured in two parts. The first part covers the exact mean-field epidemic model on temporal clique graphs, while the second part covers timescale separation and our prevalence approximation. Part one discusses the required theoretical background of NIMFA (Sec. II) and RWIG (Sec. III). Then, we deduce the exact solution of NIMFA on temporal clique graphs in Sec. IV. In part two, we first treat NIMFA on RWIG in the annealed regime and the lower transition time $\underline{\mathrm{T}}(r)$ in Sec. V and then discuss our prevalence approximation in Sec. VI. We conclude in Sec. VII.

II. *N*-INTERTWINED MEAN-FIELD APPROXIMATION

Consider a static, connected, and undirected contact graph G with N nodes and L links. The graph G is described by a symmetric adjacency matrix A, which has elements $a_{ij} = a_{ji} = 1$ if nodes i and j are connected, or $a_{ij} = a_{ji} = 0$ if nodes i and j are not connected. We consider the Markovian SIS epidemic spreading process on G, where infected nodes cure with rate δ and infect susceptible neighbors with infection rate β. The infection probability $w_i(t)$ of a node i at time t in a homogeneous Markovian SIS epidemic can be upper bounded [20] by $w_i(t) \leqslant v_i(t)$, where $v_i(t)$ is the NIMFA infection probability of node i at time t. The homogeneous NIMFA equations [20–22] are given, for each node i, by

$$\frac{\mathrm{d}\, v_i(t)}{\mathrm{d}t} = -\delta v_i(t) + \beta(1 - v_i(t)) \sum_{j=1}^{N} a_{ij} v_j(t), \qquad i = 1, 2, \ldots, N. \tag{1}$$

The set of NIMFA differential equations in Eq. (1) can be written in matrix form, denoting the infection probability vector $V(t) = [v_1(t), \ldots v_N(t)]^T$ as

$$\frac{\mathrm{d}V(t)}{\mathrm{d}t} = (\beta A - \delta I)V(t) - \beta \mathrm{diag}(V(t))AV(t), \tag{2}$$

where I is the $N \times N$ identity matrix and $\mathrm{diag}(x)$ is the diagonal matrix with the elements x_i of the $N \times 1$ vector x on the diagonal. The prevalence $y(t)$, which is the expected fraction of infected nodes, is given by

$$y_{\mathrm{SIS}}(t) = \frac{1}{N}\sum_{i=1}^{N} w_i(t), \quad y_{\mathrm{NIMFA}}(t) = \frac{1}{N}\sum_{i=1}^{N} v_i(t). \tag{3}$$

A. NIMFA on temporal networks

NIMFA can be extended to temporal networks. Given a sequence $A_1, A_2, \ldots, A_k, \ldots$ of adjacency matrices, corresponding to a sequence of graphs $G_1, G_2, \ldots, G_k, \ldots$, such that during each interval $[t_k, t_{k+1})$, the time-variant adjacency matrix $A(t)$ of the temporal network $G(t)$ equals a constant adjacency matrix A_k, the NIMFA equations [19] for the temporal network $G(t)$ are

$$\begin{aligned}
\frac{\mathrm{d}V(t)}{\mathrm{d}t} &= (\beta A_1 - \delta I)V(t) - \beta \mathrm{diag}(V(t))A_1 V(t), \quad t \in [t_1, t_2), \\
&\vdots \\
\frac{\mathrm{d}V(t)}{\mathrm{d}t} &= (\beta A_k - \delta I)V(t) - \beta \mathrm{diag}(V(t))A_k V(t), \quad t \in [t_k, t_{k+1}), \\
&\vdots
\end{aligned} \tag{4}$$

The NIMFA system in Eq. (4) is called *piecewise*, because the NIMFA equation is defined on a set of intervals during which the temporal graph $G(t)$ is fixed and static, such that on each interval the NIMFA equation is given by a possibly different function. The representation of a temporal network $G(t)$ in terms of a sequence of adjacency matrices $A_1, A_2, \ldots$ and a sequence of disjoint covering intervals $[t_k, t_{k+1})$, where the ith adjacency matrix describes the temporal network $G(t)$ om the ith interval is sometimes called the *snapshot representation* of $G(t)$. Every temporal network $G(t)$ that does not change infinitely fast has a snapshot representation. The snapshot representation allows for a piecewise definition as in Eq. (4) and, indeed, a piecewise solution of NIMFA on temporal networks with clique structure. The piecewise set (4) is central in this work.

B. Epidemic threshold

If we define the effective infection rate as $\tau = \frac{\beta}{\delta}$, then a phase transition [23] happens at the epidemic threshold $\tau = \tau_c$ in a Markovian SIS process. If the effective infection rate $\tau > \tau_c$, an epidemic will occur with high probability, while

if the effective infection rate $\tau \leqslant \tau_c$, an epidemic will die-out exponentially fast [22].

The NIMFA epidemic threshold [20,21] is precisely given by $\tau = \tau_c^{(1)} = \frac{1}{\lambda_1}$, where λ_1 is the largest eigenvalue of the adjacency matrix A. Below the epidemic threshold $\tau \leqslant \tau_c^{(1)}$, NIMFA decays to the all-healthy state $V(t) = 0$ for all nodes. Above the epidemic threshold, $\tau > \tau_c^{(1)}$, NIMFA has one stable steady state. The infection probability vector $V(t)$ converges to a nonzero steady-state vector $V_\infty = \lim_{t\to\infty} V(t)$. If the initial infection probability vector $V(0) = 0$ at time $t = 0$, the steady-state infection probability vector $V_\infty = 0$ as well, but the all-healthy steady state is unstable above the epidemic threshold.

In the simulations in this work, we will set the curing rate $\delta = 1$, such that the effective infection rate $\tau = \beta$, without loss of generality. Setting the curing rate δ to 1 is equivalent to rescaling the time t into units of the average curing time $\frac{1}{\delta}$, as shown in Refs. [19,22].

C. Exact solution of NIMFA on the complete graph

The analytic solution $V(t)$ of the NIMFA equation (2) is generally unknown. If the $N\times N$ adjacency matrix A is the $N\times N$ all-one matrix J_N, Prasse *et al.* [18] have solved the NIMFA governing equation (2), which reduces to

$$\frac{\mathrm{d}V(t)}{\mathrm{d}t} = (\beta J_N - \delta I)V(t) - \beta \mathrm{diag}(V(t))J_N V(t), \quad (5)$$

or equivalently, with the prevalence $y(t)$ in Eq. (3),

$$\frac{\mathrm{d}V(t)}{\mathrm{d}t} = -\delta V(t) + \beta N y(t)(u - V(t)),$$

where u is the $N\times 1$ all-one vector.

An adjacency matrix A that is the all-one matrix corresponds to a complete graph *with self-loops*. The complete graph with self-loops has as largest eigenvalue $\lambda_1 = N$, while all other eigenvalues are zero. On the complete graph with self-loops and any initial condition $V(0)$, the solution $V(t)$ of NIMFA in Eq. (5) is given in Theorem 4 of Ref. [18]. The solution consists of two cases: a general formula that holds everywhere except at the threshold $\tau = \frac{1}{\lambda_1} = \frac{1}{N}$ and a second formula that holds only at the threshold $\tau = \tau_c^{(1)} = \frac{1}{N}$, where $\tau N = 1$ and $\delta = \beta N$. If $\tau \neq \tau_c^{(1)} = \frac{1}{N}$, then the infection probability vector $V(t)$ is given for all t and any initial condition $V(0)$ by

$$V(t) = \frac{1}{2}\left(1 - \frac{1}{\tau N}\right)\left(1 + \tanh\left(\frac{\beta N - \delta}{2}t + \operatorname{arctanh}\left(\frac{2\tau}{\tau N - 1}u^T V(0) - 1\right)\right)\right)u + \frac{e^{-\frac{1}{2}(\beta N+\delta)t}}{\sqrt{1 - \left(\frac{2\tau}{\tau N-1}u^T V(0) - 1\right)^2}}\operatorname{sech}\left(\frac{\beta N - \delta}{2}t + \operatorname{arctanh}\left(\frac{2\tau}{\tau N - 1}u^T V(0) - 1\right)\right)V_{\mathrm{ker}}(0), \quad (6)$$

where u is the $N\times 1$ all-one vector and $V_{\mathrm{ker}}(0) = (I - \frac{1}{N}uu^T)V(0) = (V(0) - \frac{u^T V(0)}{N}u)$. At the epidemic threshold $\tau = \tau_c^{(1)} = \frac{1}{N}$, the infection probability vector $V(t)$, is, for all t and any initial condition $V(0)$, given by

$$V(t) = \left(\delta t + \frac{N}{u^T V(0)}\right)^{-1} u + \frac{N e^{-\delta t}}{\delta t u^T V(0) + N} V_{\mathrm{ker}}(0). \quad (7)$$

In Theorem 4 in Ref. [18], the exponential terms $e^{-\frac{1}{2}(\beta N+\delta)t}$ in Eq. (6) and $e^{-\delta t}$ in Eq. (7) are multiplied by $\frac{V_{\mathrm{ker}}^T(0)V(0)}{||V_{\mathrm{ker}}(0)||_2^2}$, which we have removed, because $\frac{V_{\mathrm{ker}}^T(0)V(0)}{||V_{\mathrm{ker}}(0)||_2^2}$ is always equal to one:

$$\frac{V_{\mathrm{ker}}^T(0)V(0)}{||V_{\mathrm{ker}}(0)||_2^2} = \frac{\left(V(0) - \frac{u^T V(0)}{N}u\right)^T V(0)}{\left(V(0) - \frac{u^T V(0)}{N}u\right)^T \left(V(0) - \frac{u^T V(0)}{N}u\right)} = \frac{V(0)^T V(0) - \frac{\left(u^T V(0)\right)^2}{N}}{V(0)^T V(0) - 2\frac{\left(u^T V(0)\right)^2}{N} + \frac{\left(u^T V(0)\right)^2}{N}} = 1,$$

where we have used $V(0)^T u = u^T V(0)$ and $u^T u = N$ in the second step. Additionally, we have simplified Eq. (7) by observing that the exponents τN in Theorem 4 in Ref. [18] simplify to 1 when $\tau = \tau_c^{(1)}$. We show how to find Eq. (7) by taking the limit of Eq. (6) in Appendix A 1.

III. RWIG MODEL

The RWIG model, introduced in Ref. [7], is a Markovian model for generating temporal contact graphs $G(t)$. In RWIG, M walkers move between the N locations of a shared location set $\mathcal{N}$ according to a Markovian mobility process. The colocation principle is applied, which assumes that two walkers i and j in the same location at time t are considered to be in contact at time t. The contact graph $G(t)$ has M nodes, one for each walker, and contains the links $i \sim j$ and $j \sim i$ if walkers i and j are in contact, i.e., in the same location, at time t (see Fig. 1). Because all walkers in the same location are all connected to each other and not to other walkers, the contact graph $G(t)$ is at all times a union of multiple disconnected, fully connected components. These fully connected components are called *cliques*. We will call graphs, such as the RWIG contact graph $G(t)$, which are composed of only disconnected cliques at all times t *temporal clique graphs*. The mobility process that describes the movement of the walkers in RWIG can be defined as a discrete-time or continuous-time Markov process. In discrete-time RWIG (DRWIG) [7] the single-walker mobility process of walker m is defined by the probability transition matrix P_m. The contact graph $G[k]$ is only defined at discrete times $k = 0, 1, 2 \ldots$. In continuous-time RWIG (CRWIG) [8] the single-walker mobility process of walker m is defined by the infinitesimal generator Q_m. The contact graph $G(t)$ is defined at all times $t \geqslant 0$. The infinitesimal generators Q_m and transition matrices P_m are called the *walker policies*, as they

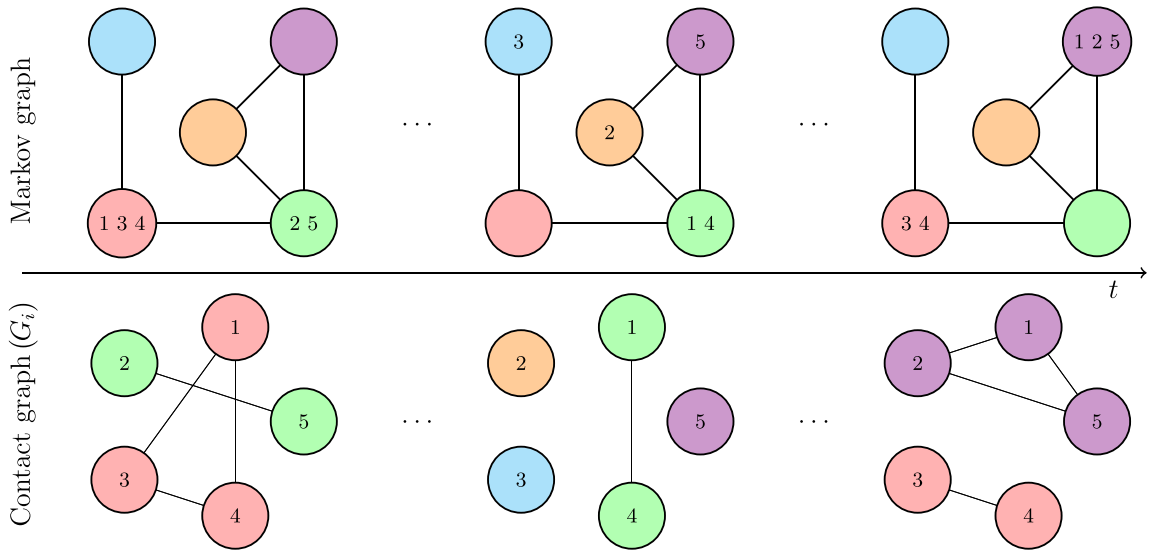


FIG. 1. Schematic illustration of the RWIG process. In the upper half $M = 5$ walkers move between the $N = 5$ locations of the Markov graph. The location of each walker is indicated in the Markov graph with their index. In the lower half the contacts between walkers are shown. The contact graph has a link between those walkers that are in the same location in the Markov graph. The location of each walker is indicated in the contact graph by the color of their node, which corresponds to the color of their location in the Markov graph.

describe the walker behavior. These walker policies are very general: RWIG is based on the beautiful fact that a random walk on a Markov graph executes a realization of that Markov process.

In this work, we will assume that DRWIG and CRWIG processes have a steady state. We denote the steady state of walker m as the $N\times 1$ vector π_m, which has elements

$$(\pi_m)_j = \lim_{t\to\infty} \Pr[\text{Walker } m \text{ is in location } j \text{ at time } t]$$

and is independent of the initial location of the walker if π_m exists. The existence of the steady state and the convergence of DRWIG and CRWIG to their steady states are treated in Ref. [8].

IV. EXACT NIMFA SOLUTION ON RWIG

We consider the NIMFA process in Eq. (4) with infection rate β and curing rate δ on the contact graph $G(t)$ generated by an RWIG process with added self-loops. We explain how the sequence of adjacency matrices $A_1, A_2, \ldots, A_k, \ldots$ and their corresponding intervals $[t_k, t_{k+1})$ are generated by a realization of an RWIG process.

If the contact graph $G(t)$ is generated by CRWIG, then the contact graph changes at (random) times $t_1 = 0, \ldots, t_k, \ldots \in \mathbb{R}$ and stays constant in between. CRWIG thus generates both the sequence of contact graphs $G_1, G_2 \ldots, G_k, \ldots$ (and, therefore, the sequence of adjacency matrices) and the corresponding intervals, such that Eq. (4) can be applied directly. If the contact graph $G(t)$ is generated with DRWIG instead, then the sequence of adjacency matrices follows from the sequence of contact graphs $G_1 = G[1], G_2 = G[2], \ldots, G_k = G[k], \ldots$. However, in DRWIG, nothing is assumed about the corresponding time-intervals. It is reasonable[1] to assume that each discrete time-step in a discrete Markov processes such as DRWIG has the same length. We will denote the length of the discrete time-step with Δt and we define the times at which the contact graph $G(t)$ changes as $t_1 = 0, t_2 = \Delta t, \ldots, t_k = (k-1)\Delta t, \ldots$. Then, Eq. (4) can be applied.

Because NIMFA on the complete graph with self-loops has been solved exactly [18], we can solve NIMFA on clique graphs with self-loops exactly as well. At all times t, NIMFA on a temporal clique graph is equal to multiple independent NIMFA epidemics, one occurring in each of the cliques, all of them solvable with Eqs. (6) and (7). We write a system of N independent epidemics, one for each location in $\mathcal{N}$. We split the infection probability vector $V(t)$ according to the cliques that exist during each interval where the contact graph $G(t)$ is static. Consider the ith interval $[t_i, t_{i+1})$, we denote with $C_j^{(i)}$ the set of walkers that are at location j during the ith interval $[t_i, t_{i+1})$. The number of walkers in location j during the ith interval is written as $M_j^{(i)} = |C_j^{(i)}|$ and the elements of $C_j^{(i)}$ are $(c_j^{(1)})_1, \ldots, (c_j^{(1)})_{M_j^{(i)}}$. We split the $M\times 1$ infection probability vector $V(t)$ into the $M_j^{(i)}(t)\times 1$ clique infection probability vectors $V_j^{(i)}(t) = [v_{(c_j^{(1)})_1}(t), \ldots, v_{(c_j^{(1)})_{M_j^{(i)}}}(t)]^T$, as illustrated in Fig. 2.

The clique infection probability vector $V_j^{(i)}(t)$ is defined for all times t because its elements, the infection probabilities $v_m(t)$, are defined at all times t. If $t \notin [t_i, t_{i+1})$, the collection of infection probabilities $v_m(t)$ does not necessarily correspond to an existing clique in the current contact graph $G(t)$. During the ith interval $[t_i, t_{i+1})$ the "full" NIMFA equation of the infection probability vector $V(t)$ on a temporal clique

[1]The Markov property says that, in a discrete Markov process $X[k]$, the transition probability $\Pr[X[k+1] = i | X[k] = j] = p_{ij}$ for all states i, j and all discrete times k, is independent of the discrete time k and suggests that all discrete steps have the same length.

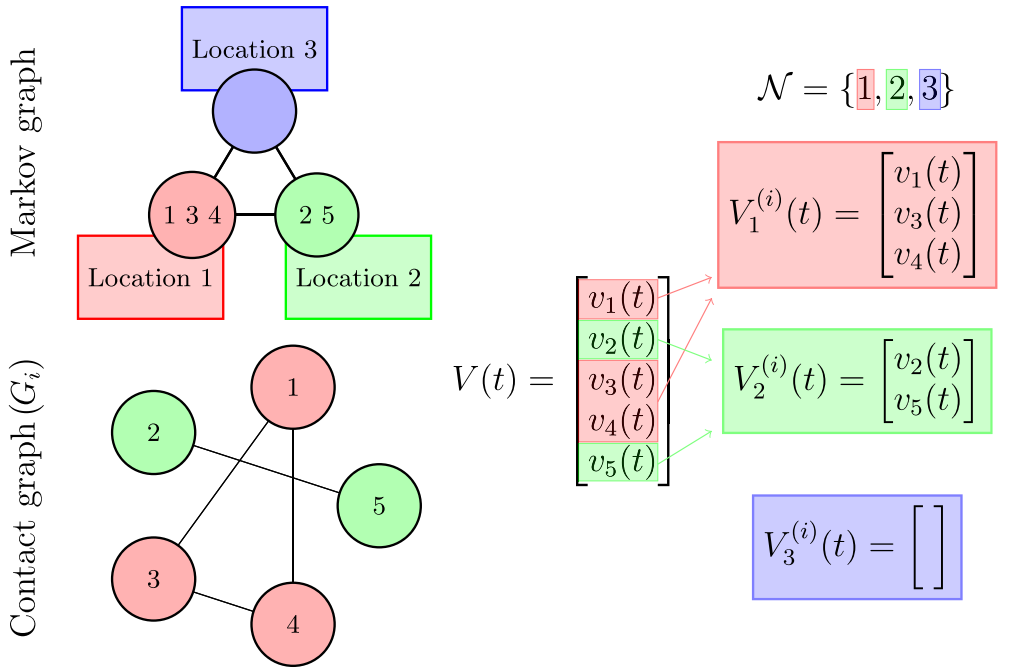


FIG. 2. Schematic visualization of the splitting of the infection probability vector $V(t)$ into the clique infection probability vectors $V_j^{(i)}(t)$ in the ith interval. The locations in the Markov graph and the walkers that are in those locations are indicated with red, green and blue for locations 1, 2, and 3, respectively.

graph with self-loops is given by

$$\frac{\mathrm{d}V(t)}{\mathrm{d}t} = (\beta A_i - \delta I)V(t) - \beta \mathrm{diag}(V(t))A_i V(t), \tag{8}$$

which we can split into the N independent clique equations for the clique infection probability vectors $V_j^{(i)}(t)$ given by

$$\begin{aligned} \frac{\mathrm{d}V_1^{(i)}(t)}{\mathrm{d}t} &= \left(\beta J_{M_1^{(i)}} - \delta I_{M_1^{(i)}}\right)V_1^{(i)}(t) - \beta \mathrm{diag}\left(V_1^{(i)}(t)\right)J_{M_1^{(i)}}V_1^{(i)}(t), \\ &\vdots \\ \frac{\mathrm{d}V_N^{(i)}(t)}{\mathrm{d}t} &= \left(\beta J_{M_N^{(i)}} - \delta I_{M_N^{(i)}}\right)V_N^{(i)}(t) - \beta \mathrm{diag}\left(V_N^{(i)}(t)\right)J_{M_N^{(i)}}V_N^{(i)}(t), \end{aligned} \tag{9}$$

where I_N and J_N are the $N \times N$ identity matrix and $N \times N$ all-one matrix, respectively.

Each of the independent equations in Eq. (9) has the shape of Eq. (5) and is solved by Eq. (6) or Eq. (7). Therefore, we obtain the solutions of Eq. (9) with as initial condition the initial infection probability vector of the interval $V(t_i)$, which contains all initial clique infection probability vectors of the interval $V_j^{(i)}(t_i)$ for the N independent equations in Eq. (9).

Theorem 1. Consider a homogeneous NIMFA process with infection rate β and curing rate δ on a time-variant contact graph that has a snapshot representation. Assume every graph in the sequence $G_1, G_2 \ldots, G_i$ is a clique graph with self-loops, such that the NIMFA process is described by Eq. (9) on each interval $[t_i, t_{i+1})$. Then, the NIMFA infection probability vector $V(t)$ can be solved piecewise by

(a) If $\tau \neq (\tau_c^{(1)})_j^{(i)} = \frac{1}{M_j^{(i)}}$, then the $M_j^{(i)} \times 1$ clique infection probability vector $V_j^{(i)}(t)$ of clique j in the interval $t \in [t_i, t_{i+1}]$ is given by

$$\begin{aligned} V_j^{(i)}(t) = &\frac{1}{2}\left(1 - \frac{1}{\tau M_j^{(i)}}\right)\left(1 + \tanh\left(\frac{\beta M_j^{(i)} - \delta}{2}(t - t_i) + \operatorname{arctanh}\left(2\frac{\tau}{\tau M_j^{(i)} - 1}u^T V_j^{(i)}(t_i) - 1\right)\right)\right)u \\ &+ \frac{e^{-\frac{1}{2}(\beta M_j^{(i)} + \delta)(t - t_i)}\operatorname{sech}\left(\frac{\beta M_j^{(i)} - \delta}{2}(t - t_i) + \operatorname{arctanh}\left(2\frac{\tau}{\tau M_j^{(i)} - 1}u^T V_j^{(i)}(t_i) - 1\right)\right)}{\sqrt{1 - \left(2\frac{\tau}{\tau M_j^{(i)} - 1}u^T V_j^{(i)}(t_i) - 1\right)^2}} V_{\mathrm{ker}}^{(i)}(t_i; j), \end{aligned} \tag{10}$$

where u is the $M_j^{(i)} \times 1$ all-one vector and $V_{\mathrm{ker}}^{(i)}(t_i; j) = (I - \frac{1}{M_j^{(i)}}uu^T)V_j^{(i)}(t_i)$.

(b) If $\tau = (\tau_c^{(1)})_j^{(i)} = \frac{1}{M_j^{(i)}}$, then the clique infection probability vector $V_j^{(i)}(t)$ is given by

$$V_j^{(i)}(t) = \left(\delta(t-t_i) + \frac{M_j^{(i)}}{u^T V_j^{(i)}(t_i)}\right)^{-1} u + \frac{M_j^{(i)} e^{-\delta(t-t_i)}}{\delta(t-t_i)u^T V_j^{(i)}(t_i) + M_j^{(i)}} V_{\text{ker}}^{(i)}(t_i; j). \tag{11}$$

Proof. Theorem 1 follows from applying Eqs. (6) and (7) to Eq. (9), since the elements of $V_j^{(i)}(t)$ describe the infection probabilities of a NIMFA process on a complete graph with $M_j^{(i)}$ nodes and self-loops as in Eq. (5). Since the interval starts at t_i and not 0, the time has to be shifted from t to $t - t_i$. Because the derivative of $v_m(t)$ of each walker m exists on the entire interval [see Eq. (4)], we know that $v_m(t)$ is continuous and that $v_m(t_i) = \lim_{\epsilon \downarrow 0} v_m(t_i - \epsilon) = \lim_{\epsilon \downarrow 0} v_m(t_i + \epsilon)$. Therefore, the solutions (10) and (11) hold on the closed interval $t \in [t_i, t_{i+1}]$. ■

In this section, we have indexed the clique infection probability vectors $V_j^{(i)}(t)$ with their location j, but if the temporal clique graph is not generated by RWIG this indexing may not be possible. However, the index j of the clique infection probability vectors $V_j^{(i)}(t)$ is arbitrary. By indexing the cliques, say from $1, \ldots, \mathcal{C}^{(i)}$, the system (9) of independent equations holds for all temporal clique graphs that have a snapshot representation. Theorem 1 solves Eq. (9), for any indexing of the cliques, and therefore, holds for all temporal clique graphs, not only those generated by RWIG.

V. ANNEALING REGIME IN NIMFA ON RWIG

The time-step Δt between network changes in DRWIG is the characteristic time (or the inter-update time [19]) of DRWIG and determines whether timescale separation is possible or not. Timescale separation allows us to simplify the network dynamics in certain cases. If the characteristic time Δt is very small compared to the characteristic times of the epidemic (i.e., the average curing time $\frac{1}{\delta}$ and average infection time $\frac{1}{\beta}$), the temporal network is accurately described by a time-averaged, static network. In order words, the dynamic process experiences the temporal network as if it was equal to its time-average: $A(t) \approx \lim_{T\to\infty} \frac{1}{T}\int_0^T A(u)du$, at all times t. However, if the characteristic time Δt is very large compared to those of the epidemic, then the network can be assumed static. In both cases the temporal dynamics can be ignored, either by averaging the temporal network or by ignoring the dynamics.

As a function of the characteristic time Δt, we can identify three regimes: (i) the annealed regime, where the network changes fast compared to the epidemic and the time-average approximation is accurate, (ii) the quenched regime where the network changes slow compared to the epidemic and the static approximation is accurate and finally, and (iii) the intermediate regime, where the network and epidemic evolve on comparable timescales and timescale separation does not apply. The time-average and static approximations are only exact in the limits $\Delta t \to 0$ and $\Delta t \to \infty$.

The upper- and lower *transition times* $\overline{\mathrm{T}}(r)$ and $\underline{\mathrm{T}}(r)$ are defined [19] as the boundaries between the three regimes. If $\Delta t < \underline{\mathrm{T}}(r)$, then the process is in the annealed regime; if $\underline{\mathrm{T}}(r) < \Delta T < \overline{\mathrm{T}}(r)$, then the process is in the intermediate regime; and if $\Delta t > \overline{\mathrm{T}}(r)$, then the process is in the quenched regime. The transition times are functions of the *accuracy tolerance* r, which determines the accuracy of the time-average (annealed) and static (quenched) approximation for $\Delta t = \underline{\mathrm{T}}(r)$ and $\Delta t = \overline{\mathrm{T}}(r)$, respectively. Persoons *et al.* [19] evaluate the transition from the intermediate to the quenched regime, but not the transition from the intermediate to the annealed regime. In this section, we show that the exact time-average of RWIG is known, which allows us to define and investigate the lower transition time $\underline{\mathrm{T}}(r)$ afterwards.

A. Multigroup multipatch SIS model

Bichara *et al.* [24] introduce the multigroup multipatch (MGMP) SIS model. In our notation, the MGMP model considers M individuals divided over R groups that move between N patches. Each member of group i spends a fraction of time p_{ij} in patch j. Patches in MGMP are conceptually equivalent to locations between which the walkers move in RWIG. Patches, like locations in RWIG, describe locations/activities/events, where contacts between individuals occur and infections may happen. The (time-averaged) contact dynamics are encoded in the residence-time matrix P. The residence-time matrix P, with elements p_{ij}, describes which fraction of time members from each group are in each patch. The main motivation of MGMP is that the residence-time matrix P is easier to measure through surveys than, for example, a contact graph or human mobility patterns. The MGMP governing equation is given by

$$\frac{\mathrm{d}\, I_i(t)}{\mathrm{d}t} = -\delta_i I_i(t) + \sum_{j=1}^{N} \beta_j S_i(t) p_{ij} y_j(t), \tag{12}$$

where $I_i(t)$ and $S_i(t)$ are the number of infectious and susceptible individuals in group i respectively and $y_j(t)$ is the prevalence of the individuals in patch j. The curing rate δ_i and infection rate β_j are group- and patch-dependent, respectively.

The MGMP model (12) enables time-averaging of NIMFA on RWIG. Indeed, consider the R groups as groups of walkers with the same policy and then equate $p_{ij} = (\pi_m)_j$, where $(\pi_m)_j$ is the probability that a walker m from group i is in location j in the RWIG steady state. The mean-field infection probability $v_i(t)$ in NIMFA corresponds to $\frac{I_i(t)}{N}$, where each group i has size $N_i = 1$, i.e., $R = M$.

If we assume homogeneous curing rates $\delta_i = \delta$ and assume that $\beta_j = \theta_j \beta$, Eq. (12) becomes

$$\frac{\mathrm{d}\, v_i(t)}{\mathrm{d}t} = -\delta v_i(t) + \beta \sum_{j=1}^{N} p_{ij}\theta_j (1 - v_i(t)) y_j(t).$$

After substituting $\sum_{i=1}^{R} p_{ij} = \sum_{k=1}^{M} p_{kj} = \theta_j$, we find that

$$\frac{\mathrm{d}\, v_i(t)}{\mathrm{d}t} = -\delta v_i(t) + \beta(1 - v_i(t)) \sum_{k=1}^{M} \left(\sum_{j=1}^{N} p_{ij} p_{kj}\right) v_k(t),$$

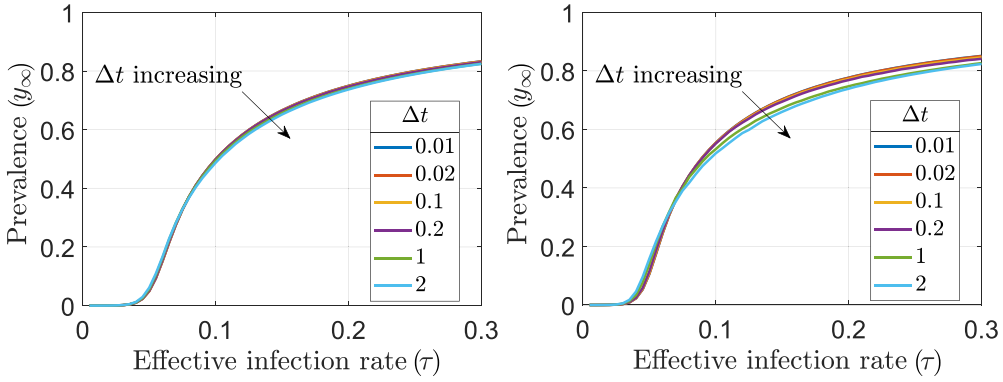


FIG. 3. Steady-state prevalence of NIMFA on DRWIG as a function of the effective infection rate τ for various values of the time step Δt. The baseline parameters from Appendix B 1 are used. Left: ER-policies; Right: BA-policies.

which is NIMFA on the graph with link weights $a_{ik} = \sum_{j=1}^{N} p_{ij}p_{kj}$. As explained below, we must exclude that $k = i$ to arrive, after substitution of $p_{ij} = (\pi_i)_j$, at

$$\frac{\mathrm{d}\, v_i(t)}{\mathrm{d}t} = -\delta v_i(t) + \beta(1 - v_i(t)) \sum_{k=1,k\neq i}^{M} \left(\sum_{j=1}^{N} (\pi_i)_j (\pi_k)_j \right) v_k(t). \tag{13}$$

The time-average approximation (13) is exact in the annealed limit because the steady-state probability of a state in a Markov chain is also the fraction of time the process spends in that state given infinite time. The time average of the link a_{ik}, given by $\lim_{T\to\infty} \frac{1}{T} \int_0^T a_{ik}(u)du$ is thus equal to the fraction of time the link a_{ik} exists, which is equal to the fraction of time the process spends in a state where both walkers i and k are in the same location. The fraction of time the process spends in a state where both walkers i and k are in the same location is in turn given by the probability that walkers i and k are in the same location in the steady state, which is $\sum_{j=1}^{N} (\pi_i)_j (\pi_k)_j$. Since we exclude self-loops in NIMFA, $a_{ii}(t) = 0$ at all times t, for all walkers i and the time-average $\lim_{T\to\infty} \frac{1}{T} \int_0^T a_{ii}(u)du = 0$. Therefore, the diagonal elements $a_{ii} = 0 \neq \sum_{j=1}^{N} (\pi_i)_j^2$ have to be excluded.

We conclude that, when NIMFA on RWIG is annealing, the residence-time matrix P contains all mobility data required for an accurate description of the epidemic.

B. Lower transition time

Since Eq. (13) is exact in the annealed limit, Eq. (13) only approximates the process in the annealed regime. As in Ref. [19], we assume in the DRWIG process that the time between changes in the network is constant and equal to Δt. The lower transition time $\underline{\mathrm{T}}(r)$, as a function of the accuracy tolerance r, describes whether or not the temporal network is in the annealed regime. For fixed NIMFA and RWIG parameters, we define the lower transition time as

$$\underline{\mathrm{T}}(r) = \underset{\Delta t \geqslant 0}{\operatorname{argmax}} \{ |y_\infty(\Delta t) - \tilde{y}_\infty| \leqslant r \}, \tag{14}$$

where the steady-state prevalence of Eq. (13) is denoted $\tilde{y}_\infty$ and $y_\infty(\Delta t)$ is the expected steady-state prevalence of NIMFA on RWIG for a given value of the time-step Δt. If the time-step $\Delta t \leqslant \underline{\mathrm{T}}(r)$, we are in the annealed regime, which means that the approximation (13) is accurate, according to Eq. (14).

Our definition (14) is possible because the expected steady-state prevalence y_∞ of NIMFA on RWIG varies with the time-step Δt. This critical insight was found numerically. Figure 3 shows, for different values of the time-step Δt, the expected steady-state prevalence of NIMFA on DRWIG y_∞ as a function of the effective infection rate τ. For most values of the effective infection rate τ, the steady-state prevalence is strictly increasing or decreasing. When the effective infection rate $\tau \approx 0.075$ the steady-state prevalence y_∞ does not change with the time-step Δt. This implies that either our definition (14) does not accurately distinguish annealing behavior for $\tau \approx 0.075$, or that, for this value of the effective infection rate τ, the approximation (13) describes the expected steady-state prevalence accurately for all time-steps $\Delta t \leqslant 2$. Figure 3 shows both ER- and BA-policies. Because ER-policies create cliques of equal size, while BA-policies create cliques of different sizes, the sensitivity of the prevalence to variation in Δt is amplified for BA-policies, because the viral state of the walkers is less homogeneous. Movements of walkers with higher infection probability to cliques with lower infection probability as well as movements of walkers with lower infection probability to cliques with higher infection probability will both increase the prevalence in the short term. Figure 3 implies that the annealing limit is not a general upper-bound for the steady-state prevalence $y_\infty(\Delta t)$. Between the threshold and $\Delta t \approx 0.075$ the annealing limit is a lower-bound for the steady-state prevalence $y_\infty(\Delta t)$. This regime corresponds to cases where a significant number of cliques, but not all, are below the epidemic threshold for large fractions of time.

VI. PREVALENCE APPROXIMATION

The solution of NIMFA on RWIG, given by Theorem 1, has some practical limitations. The solution in Eqs. (10) and

(11) is a piecewise and recursive formula. The solution for interval $i-1$ is needed to calculate the initial condition for interval i. To calculate the initial condition for interval $i-1$ the solution for interval $i-2$ is needed and so on. Eventually, the entire realization of the RWIG process is required. The entire sequence of contact graphs $G_1, G_2, \ldots$ and, in case of CRWIG, the transition times $t_1, t_2, \ldots$ must be known to apply Eqs. (10) and (11).

Here, we derive a closed form approximation for the prevalence $y(t)$ of NIMFA on a temporal clique graph generated by RWIG. This approximation will be a function of only the infection parameters, the infection rate β and curing rate δ, the RWIG parameters, the number of walkers M, the number of locations N and the steady-state clique-size vector Θ of the RWIG process. In the steady state, the expected number of walkers in location j is denoted by $\theta_j = \sum_{i=1}^{M}(\pi_i)_j$. The steady-state clique-size vector is thus given by $\Theta = [\theta_1, \ldots, \theta_N]$. After a series of approximations, explained below one by one, we derive the approximated prevalence $\hat{y}(t)$ given by:

Proposition 1. The prevalence of a NIMFA epidemic with infection rate β and curing rate δ, on a contact graph generated by an RWIG process with M walkers, N locations and steady-state clique-size vector $\Theta = [\theta_1, \ldots, \theta_N]$ can be approximated as

$$\hat{y}(t) = \frac{1}{M}\sum_{j=1}^{N} \frac{\theta_j \hat{y}_{j,\infty}}{1 + \left(\frac{\hat{y}_{j,\infty}}{y(0)} - 1\right)e^{-(\beta\theta_j - \delta)t}}, \tag{15}$$

where $\hat{y}_{j,\infty} = 1 - \frac{1}{\tau\theta_j}$ is the approximated steady-state clique prevalence in Eq. (22).

If the steady-state clique sizes $\theta_1, \ldots, \theta_N$ are integers, our prevalence approximation (15) is the exact solution of a NIMFA epidemic with infection rate β and curing rate δ with initial prevalence $y(0)$ on a *static network* with N cliques of sizes $\theta_1, \ldots, \theta_N$ with self-loops.

A. Set of approximations in Proposition 1

We now derive our closed-form prevalence approximation (15) step by step. In the following, we will call a vector *homogeneous* if its elements are similar and *heterogeneous* if its elements are varied. We first make two technical approximations.

Approximation I. We assume that the contact graph has self-loops, to apply our extensions (10) and (11) of the results from Prasse *et al.* [18]. Self-loops model "background" infections, e.g., infections due to aerosols or otherwise contaminated surfaces. However, adding self-loops is a non-standard way of considering background infections. The introduction of an ε-process, which causes spontaneous infections with rate ε, resulting in an ε-SIS epidemic process [22] is more common. One reason why ε-SIS is preferred over self-loops is that the background infection term $\varepsilon(1 - v_i(t))$ decreases linearly with the infection probability $v_i(t)$, while in the case of a self-loop, the background infection term $\beta v_i(t)(1 - v_i(t))$ is a parabola with maximum at $v_i(t) = \frac{1}{2}$, which is zero when the infection probability $v_i(t)$ is zero. The latter does not correspond with the physics of a realistic background infection process.

Approximation II. Since Eq. (11) only holds at the epidemic threshold $\tau = \tau_c^{(1)}$ and Eq. (10) holds in all other cases, we assume that the epidemic will generally not be exactly at the epidemic threshold $\tau = \tau_c^{(1)}$ and only Eq. (10) is used to approximate the prevalence.

These first two approximations are technical and of minor impact. By considering the clique prevalence $y_j^{(i)}(t)$ instead of the clique infection probability vector $V_j^{(i)}(t)$, Eq. (10) simplifies. The clique prevalence $y_j^{(i)}(t) = \frac{u^T V_j^{(i)}(t)}{M_j^{(i)}}$ is given by the piecewise form

$$y_j^{(i)}(t) = \frac{1}{2}\left(1 - \frac{1}{\tau M_j^{(i)}}\right)\left(1 + \tanh\left(\frac{\left(\beta M_j^{(i)} - \delta\right)}{2}(t - t_i) + \operatorname{arctanh}\left(\frac{2y_j^{(i)}(t_i)}{1 - \frac{1}{\tau M_j^{(i)}}} - 1\right)\right)\right), \tag{16}$$

which is derived in Appendix A 2. The recursive form in Eq. (16) can be solved if $M_j^{(i)}$ and $V_j^{(i)}$ are independent of i, which requires two strong approximations.

Approximation III. In the RWIG steady state, the number of walkers in each location j fluctuates around the expected number of walkers in the steady state $\theta_j = \sum_{i=1}^{M}(\pi_i)_j$ with relatively low variance due to Kolmogorov's law [25], also known as the strong law of large numbers. It is known that these fluctuations are Gaussian. Additionally, the RWIG steady state is reached exponentially fast [8]. Therefore, we assume that the contact network is in the steady state and that the number of nodes in each clique is close to its average[2]: $M_j^{(i)} \approx \theta_j$ for all intervals i.

Approximation IV. The approximation, $V_j^{(i)}$ is constant in i, implies that the contact network is approximately static, which is accurate if walkers stay significantly more stationary than that they move or if the number of walkers in each location is very large. We assume that walkers stay in the same location, such that, in combination with approximation III, the contact graph is reduced to a static graph with N disconnected cliques with sizes of approximately $\theta_1, \ldots, \theta_N$.

Approximations I, II, III, and IV simplify the solution (10) into a closed-form approximation. By applying approximations III and IV to Eq. (16), we find an approximated clique prevalence $\hat{y}_j(t)$, independent of the intervals $[t_i, t_{i+1})$ and of the graph sequence $G_1, \ldots, G_k, \ldots$. We write $V_j^{(i)}(t) = V_j(t)$, because the walkers are assumed to be in the same location at all times t and thus $y_j^{(i)}(t) = y_j(t)$. We substitute $M_j^{(i)} \approx \theta_j$ into Eq. (16) for each clique and define the initial clique prevalence $y_j(0) = \frac{u^T V_j(0)}{\theta_j}$, which yields an approximated clique prevalence $\hat{y}_j(t)$:

$$\hat{y}_j(t) = \frac{1}{2}\left(1 - \frac{1}{\tau\theta_j}\right)\left(1 + \tanh\left(\frac{(\beta\theta_j - \delta)}{2}t + \operatorname{arctanh}\left(\frac{2y_j(0)}{1 - \frac{1}{\tau\theta_j}} - 1\right)\right)\right). \tag{17}$$

[2]The steady-state clique sizes θ_j are generally not integers.

If the initial clique prevalence $y_j(0) = 0$, then Eq. (17) reduces to $\hat{y}_j(t) = 0$ at all times t. In the exact model, an epidemic may still spread in clique j, even if the initial prevalence $y_j(0) = 0$, when the movement of the walkers introduces the epidemic into clique j and clique j is large enough to be above the epidemic threshold. If the initial clique prevalence $y_j(0) = 0$, then Eq. (17) tells us that no epidemic can start in clique j under our approximations. We repair that situation by making another approximation.

Approximation V. A nonzero infection probability $v_j > 0$ in NIMFA will lead to a nonzero infection probability $v_i > 0$ in an infinitesimally short time in a connected graph. Hence, we may assume that an epidemic starts in each location at $t = 0$. Any movement from an infected clique to a healthy clique will start the NIMFA process in the healthy clique instantaneously. If the number of walkers M is large enough and movements are frequent, all walkers m should possess nonzero infection probabilities $v_m(t) > 0$ very fast. Therefore, we require that the initial clique prevalence $y_j(0) > 0$ in all locations j; otherwise, Eq. (17) leads to no infection in location j under our assumptions. Since the initial clique prevalence $y_j(0) = \frac{u^T V_j(0)}{\theta_j}$ could be zero in general, we replace the initial clique prevalence $y_j(0)$ with the approximated initial clique prevalence $\hat{y}_j(0) > 0$.

After replacing in Eq. (17) the exact initial prevalence $y_j(0)$ by the approximated initial prevalence $\hat{y}_j(0)$, we obtain

$$\hat{y}_j(t) = \frac{1}{2}\left(1 - \frac{1}{\tau\theta_j}\right)\left(1 + \tanh\left(\frac{(\beta\theta_j - \delta)}{2}t + \operatorname{arctanh}\left(\frac{2\hat{y}_j(0)}{1 - \frac{1}{\tau\theta_j}} - 1\right)\right)\right). \quad (18)$$

We complement Eq. (18) with Eq. (3) to find our approximation $\hat{y}(t)$ of the prevalence in the entire contact graph as

$$\hat{y}(t) = \frac{1}{M}\sum_{j=1}^{N} \theta_j \hat{y}_j(t). \quad (19)$$

Our approximation $\hat{y}(t)$ in Eqs. (19) and (18) depends on the NIMFA parameters (the curing rate δ and the infection rate β), the RWIG parameters (the number of walkers M, the number of locations N and the expected steady-state clique-size vector $\Theta = [\theta_1, \ldots, \theta_N]$) and the approximated initial clique prevalence $\hat{y}_j(0)$. It remains to fix $\hat{y}_j(0) > 0$ for each clique j by assuming a homogeneous initial infection probability vector.

Approximation VI. We set the approximated initial clique prevalence $\hat{y}_j(0) = \frac{u^T V(0)}{M} = y(0)$ for all cliques j, which implies an equal initial condition for all walkers.[3]

In Eq. (18), we replace $\hat{y}_j(0)$ by $y(0)$ and the approximated steady-state clique prevalence $\hat{y}_{j,\infty} = 1 - \frac{1}{\tau\theta_j}$, which is derived in Eq. (22), and finally arrive at

$$\hat{y}_j(t) = \frac{\theta_j \hat{y}_{j,\infty}}{2}\left(1 + \tanh\left(\frac{\beta\theta_j - \delta}{2}t + \operatorname{arctanh}\left(2\frac{y(0)}{\hat{y}_{j,\infty}} - 1\right)\right)\right). \quad (20)$$

In Appendix A 3, we rewrite Eq. (20) as

$$\hat{y}_j(t) = \frac{\hat{y}_{j,\infty}}{1 + \left(\frac{\hat{y}_{j,\infty}}{y(0)} - 1\right)e^{-(\beta\theta_j - \delta))t}}. \quad (21)$$

After substituting the approximated clique prevalence (21) into Eq. (19), we obtain our approximation (15). ■

B. Steady state of the prevalence approximation

The approximated steady-state clique prevalence $\hat{y}_{j,\infty}$ in a clique of size θ_j with self-loops in Eq. (21) is equal to

$$\hat{y}_{j,\infty} = \lim_{t\to\infty} \frac{1}{2}\left(1 - \frac{1}{\tau\theta_j}\right)\left(1 + \tanh\left(\frac{\beta\theta_j - \delta}{2}t + \operatorname{arctanh}\left(\frac{2\tau\theta_j\hat{y}_j(0)}{\tau\theta_j - 1} - 1\right)\right)\right) = 1 - \frac{1}{\tau\theta_j}, \quad (22)$$

because $\lim_{t\to\infty} \tanh(t) = 1$, which only applies to Eq. (22) above the threshold,[4] i.e., if $\beta\theta_j - \delta > 0$. The steady-state prevalence $1 - \frac{1}{\tau\theta_j}$ is independent of the initial condition, as long as $y_j(0) > 0$ and holds also without approximation VI. Because $1 - \frac{1}{\tau\theta_j} = 0$ at the clique epidemic threshold $\tau\theta_j = 1$ and is negative below the clique epidemic threshold, the approximated steady-state clique prevalence is given by

$$\hat{y}_{j,\infty} = \max\left\{0, 1 - \frac{1}{\tau\theta_j}\right\}.$$

An elegant formula for the approximated steady-state prevalence $\hat{y}_\infty$ in Eq. (19) can be derived from Eq. (22) if all cliques j are above the epidemic threshold:

$$\hat{y}_\infty = \frac{1}{M}\sum_{j=1}^{N}\theta_j\hat{y}_{j,\infty} = \frac{1}{M}\sum_{j=1}^{N}\left(\theta_j - \frac{1}{\tau}\right) = \frac{\sum_{j=1}^{N}\theta_j}{M} - \frac{N}{M\tau} = 1 - \frac{1}{\tau\rho}, \quad (23)$$

where $\sum_{j=1}^{N}\theta_j = \sum_{j=1}^{N}\sum_{i=1}^{M}(\pi_i)_j = \sum_{i=1}^{M}\sum_{j=1}^{N}(\pi_i)_j = \sum_{i=1}^{M} 1 = M$ and where the *walker density* $\rho = \frac{M}{N}$ is introduced.

Interestingly, the approximated steady-state prevalence (23) is independent of the expected steady-state clique size vector Θ and thus independent of the RWIG process! The approximated steady-state prevalence $\hat{y}_\infty = 1 - \frac{N\delta}{M\beta}$ only depends on the four major parameters of NIMFA on RWIG: the curing rate δ, the infection rate β, the number of walkers M, and the number of locations N.

[3] Alternative approximated initial conditions were considered, but did not yield better results than the homogeneous initial condition of approximation VI.

[4] Below the threshold $\beta\theta_j - \delta < 0$, we apply $\lim_{t\to\infty}\tanh(-t) = -1$ to Eq. (22) such that $\hat{y}_{j,\infty} = 0$ for all j and thus $\hat{y}_\infty = 0$ as expected.

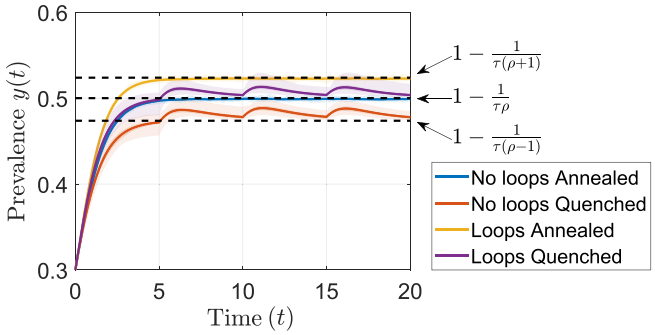


FIG. 4. Comparison of the steady states of NIMFA with and without self-loops in the annealed and quenched regime. The light-shaded area shows 100% of simulations, while the dark-shaded area shows the 50% of simulations closest to the mean (thick line). The three steady-state values as hypothesized above are shown in dashed black. The baseline parameters as described in Appendix B 1 are used with the exception of $K = 200$ and $\Delta t = 0.1$ for annealed and $\Delta t = 5$ for quenched.

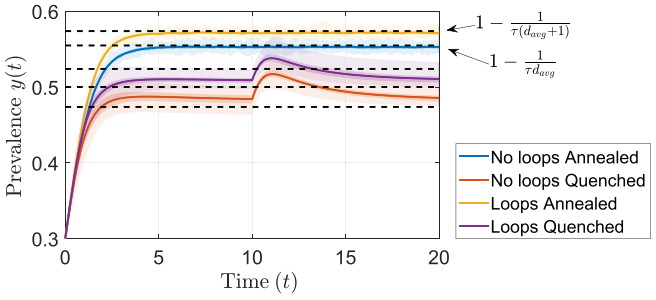


FIG. 5. Comparison of the steady states of NIMFA with and without self-loops in the annealed and quenched regime. The light-shaded area shows 100% of simulations, while the dark-shaded area shows the 50% of simulations closest to the mean (thick line). The three steady-state values from Fig. 4, as well as those with the average degree substituted, are shown in dashed black. The baseline parameters as described in Appendix B 1 are used with the exception of BA walker policies, $K = 200$ and $\Delta t = 0.1$ for annealed and $\Delta t = 5$ for quenched.

Equation (22) also follows from the known result [22] for regular graphs with degree r that the NIMFA steady-state prevalence $y_\infty = 1 - \frac{1}{\tau r}$. While our approximation assumes a static network in the RWIG steady state, the steady state (23) resembles that of an time-average, where the average degree $d_{\text{avg}} \approx \rho$ for all walkers. The physics of our assumption suggest that our approximation describes a quenched system, while the mathematical expression (23) for the approximated steady state $\hat{y}_\infty$ suggest an annealed system. We argue that our approximation describes both an quenched *and* an annealed system at the same time. This is an artifact from our first assumption: the presence of self-loops. Figure 4 shows that the approximate steady state $\hat{y}_\infty = 1 - \frac{1}{\tau\rho}$ describes the steady state of the annealed regime *without* self-loops and seemingly lower bounds the quenched regime *with* self-loops. While we are not interested in the process with self-loops, we can use its quenched steady state to find the quenched steady state of the process without self-loops. By observing that the average degree of the system with self-loops is exactly 1 higher than without self-loops, we can subtract 1 from $d_{\text{avg}} = \rho$ to find the quenched steady state without self-loops. Similarly, for completeness, we can add 1 to the average degree to find the annealed steady state of the process with self-loops. Figure 4 shows both shifted curves $1 - \frac{1}{\tau(\rho+1)}$ and $1 - \frac{1}{\tau(\rho-1)}$ and confirms their accuracy.

C. Influence of the walker policies

The walker policies are discussed and analyzed numerically in Appendix B 2 b. The simulations in Fig. 4 have used ER-policies. ER-policies have an approximately homogeneous steady state $\pi_i = \frac{1}{N}u$ for all walkers i, when N is large, such that $d_{\text{avg}} \approx \rho$. Indeed, since $(\pi_i)_j = \frac{1}{N}$ for all walkers i and locations j, the average degree is $d_{\text{avg}} \approx d_i \approx \sum_{k=1}^{M}\sum_{j=1}^{N}(\pi_i)_j(\pi_k)_j = \sum_{k=1}^{M}\sum_{j=1}^{N}\frac{1}{N^2} = \frac{M}{N} = \rho$.

For general walker policies, our assumptions that led to Proposition 1 are less accurate. The more general

$$d_{\text{avg}} = \frac{1}{M}\sum_{i=1}^{M}\sum_{k=1}^{M} a_{ik},$$

where we sum over all links, can be simplified after substitution of a_{ik} with the exact time average. Starting with

$$d_{\text{avg}} \approx \frac{1}{M}\sum_{i=1}^{M}\sum_{k=1}^{M}\sum_{j=1}^{N}(\pi_i)_j(\pi_k)_j,$$

where the expression is now approximate because we do not exclude the case where $i = k$, we change the order of the summations such that we can substitute the steady-state clique size θ_j. We have

$$d_{\text{avg}} \approx \frac{1}{M}\sum_{j=1}^{N}\left(\sum_{i=1}^{M}(\pi_i)_j\right)\left(\sum_{k=1}^{M}(\pi_k)_j\right) = \frac{1}{M}\sum_{j=1}^{N}\theta_j^2,$$

which simplifies to ρ when $\theta_j = \rho$ for all locations j, such as in ER-policies. Figure 5 considers RWIG with BA-policies. The three lines from Fig. 4, based on the walker density ρ are shown and two lines based on the average degree $d_{\text{avg}} = \frac{1}{M}\sum_{j=1}^{N}\theta_j^2$ are shown as well. The BA-policies do indeed require the modified annealed steady state $1 - \frac{1}{\tau d_{\text{avg}}}$, but the lower bound of the quenched steady state is seemingly unchanged. In Appendix B we investigate a modification to our prevalence approximation (15), where we replace the effective infection rate τ with an corrected effective infection rate $\tau_{\text{cor}} = \frac{\tau d_{\text{avg}}}{\rho}$ such that the steady-state prevalence $\hat{y}_\infty = 1 - \frac{1}{\tau d_{\text{avg}}}$. Simulations show that the estimates above are inadequate when a significant fraction of cliques is below the threshold. When a significant fraction of cliques is below the threshold, the prevalence y_∞ increases with Δt (as in Fig. 3). With many cliques below the threshold, movements can decrease the prevalence, because walkers lose their infectivity faster in the small cliques than that walkers increase their infectivity in the large cliques.

D. Heuristic proposal for lower transition time $\underline{T}(r)$

The simulations in Secs. VI B and VI C suggest that if all cliques j are above the threshold the steady-state prevalence in the annealed regime can be approximated as

$$\lim_{\Delta t\to 0} y_\infty = 1 - \frac{1}{\tau d_{\text{avg}}}, \tag{24}$$

while in the quenched regime, simulations suggest that the steady-state prevalence can be lower bounded by

$$\lim_{\Delta t\to \infty} y_\infty \geqslant 1 - \frac{1}{\tau(\rho-1)}. \tag{25}$$

Between the limit cases (24) and (25), the steady-state prevalence y_∞ is a function $f(\Delta t)$ of the time-step Δt. We cannot derive the analytic form $f(\Delta t)$, but simulations suggest a simple exponential decay as

$$f_\mu(t) = f(\infty) + (f(0) - f(\infty))e^{-\mu t},$$

in which μ is a tuning parameter. We find after substituting our bounds (24) and (25)

$$f_\mu(\Delta t) = 1 - \frac{1}{\tau(\rho-1)} + \left(\frac{1}{\tau(\rho-1)} - \frac{1}{\tau d_{\text{avg}}}\right)e^{-\mu\Delta t}.$$

The lower transition time $\underline{T}(r)$ in Eq. (14) is, assuming the steady-state prevalence $y_\infty(\Delta t)$ is monotonous in Δt, the solution of the inequality $|y_\infty(\underline{T}(r)) - \tilde{y}_\infty| = r$. By solving instead the equality $|f_\mu(\underline{T}(r)) - \tilde{y}_\infty| = r$, we can obtain an analytical approximation of the lower transition time $\underline{T}(r)$. Since $f_\mu(\underline{T}(r)) \leqslant \tilde{y}_\infty = 1 - \frac{1}{\tau d_{\text{avg}}}$, we can resolve the absolute value and find

$$r = \frac{1}{\tau d_{\text{avg}}} + \frac{1}{\tau(\rho-1)} - \left(\frac{1}{\tau(\rho-1)} - \frac{1}{\tau d_{\text{avg}}}\right)e^{-\mu\underline{T}(r)},$$

which yields, after some rewriting, a proposal for the lower transition time

$$\underline{T}(r) = \frac{1}{\mu}\left(\log\left(\frac{1}{\tau(\rho-1)} - \frac{1}{\tau d_{\text{avg}}}\right) - \log\left(\frac{1}{\tau d_{\text{avg}}} + \frac{1}{\tau(\rho-1)} - r\right)\right). \tag{26}$$

E. Accuracy of the prevalence approximation

Because the prevalence approximation (15) can describe both annealing and quenched processes, it is potentially accurate for a wide range of time-steps Δt. Appendix B contains an extensive numerical analysis in the form of a variation of parameters from a baseline. We summarize the simulations:

(1) NIMFA on RWIG seems to have, around our baseline parameters, very low variance in the prevalence for different RWIG realizations, even when $\Delta t = 0.5$, which is too large for the network to be annealing. This suggests the low variance of the prevalence is caused by another phenomenon, such as the homogeneous behavior of the walkers.

(2) NIMFA on DRWIG and CRWIG with equivalent policies behave surprisingly similar.

(3) The convergence of the RWIG process towards the steady state, before starting the epidemic, does not have any effect on the prevalence of the epidemic.

(4) The accuracy of our prevalence approximation (15), which in the steady state is an annealing approximation of NIMFA without self-loops, is surprisingly good under the baseline conditions used in Appendix B, even when $\Delta t = 0.5$, a value too large for RWIG to be annealing.

(5) When our prevalence approximation (15) accurately predicts the steady-state prevalence, also the transient regime is well covered.

(6) The prevalence approximation (15) performs poorly at low walker densities ρ and small numbers of initially infected walkers K.

(7) The correction $\tau \to \tau_{\text{cor}} = \frac{\tau d_{\text{avg}}}{\rho}$, as suggested in Sec. VI C, improves the accuracy of the prevalence approximation (15) when $d_{\text{avg}} \neq \rho$.

VII. CONCLUSION

To the few exact results on epidemics in temporal networks, we add the exact solution in Theorem 1 of NIMFA epidemics on temporal clique graphs with self-loops by extending the solution from Ref. [18]. The exact solution is reworked in a sequence of assumptions to an analytic closed-form approximation (15) of the NIMFA prevalence in temporal clique graphs. The approximation (15) is a function of the number of walkers M, the walker policy size N, the expected steady-state clique size Θ, the infection rate β, the curing rate δ, and the initial prevalence $y(0)$.

We evaluate the approximation (15) and show that, with an corrected effective infection rate $\tau_{\text{cor}} = \frac{d_{\text{avg}}}{\rho}$, our approximation (15) accurately predicts the steady-state prevalence in the annealed regime above the threshold. While the approximation (15) rather interpolates between an initial condition and a steady state, the approximation (15) is remarkably accurate for all times t, in those cases where the steady state is predicted accurately. For metapopulation or RWIG models with large amounts of individuals per location, our approximation (15) provides a good first order estimate at an almost vanishing computational cost (compared to simulations).

We lay the foundations for an investigation as in Ref. [19], by observing that the steady-state prevalence y_∞ changes with the step size Δt. This allows us to define the lower transition time $\underline{T}(r)$ formally. Using our prevalence approximation we also propose a methodology to analytically approximate the lower transition time $\underline{T}(r)$. The simulations required to perform a full investigation are computationally intensive and are therefore left for future work.

Some general insights were also gained. First, we learned that in some cases, specifically with ER policies, the variation around the mean prevalence of NIMFA on different realizations of the same RWIG process is small, even in the quenched regime, as shown in Fig. 4, where the dark-shaded area, which covers 50% of the simulations, is almost indistinguishable from the mean. Second, we found that the initial condition of the RWIG process has negligible effect on the epidemic, which is a curious result. It is known [8] that RWIG converges exponentially fast to the steady state; however, during the first period of the epidemic the distribution of the walkers still includes some influence of the initial condition.

ACKNOWLEDGMENTS

We thank Brian L. Chang for his contribution of simulation results in this article. We thank the reviewers for their helpful comments, which have improved this work. This research has been funded by the European Research Council (ERC) under the European Union's Horizon 2020 research and innovation programme (Grant Agreement No. 101019718).

DATA AVAILABILITY

There are no publicly available research data or software. Data that support the findings of this article are available from the authors upon reasonable request.

APPENDIX A: DERIVATIONS

1. Derivation of Eq. (7) from Eq. (6)

We derive Eq. (7) from Eq. (6) by taking the limit $\tau \to \tau_c^{(1)} = \frac{1}{N}$. Starting with Eq. (6), we define $\varepsilon = \tau N - 1$ and $w = \frac{2\tau}{\tau N - 1} u^T V(0) - 1$. After substitution we have

$$V(t) = \frac{1}{2}\frac{\varepsilon}{\tau N}\left(1 + \tanh\left(\frac{\varepsilon\delta}{2}t + \operatorname{arctanh}(w)\right)\right)u + \frac{e^{-\delta t}}{\sqrt{1-w^2}}\operatorname{sech}\left(\frac{\varepsilon\delta}{2}t + \operatorname{arctanh}(w)\right)V_{\ker}(t).$$

Before taking the limit we rewrite the tanh and sech functions using the identities

$$\tanh(x+y) = \frac{\tanh(x) + \tanh(y)}{1 + \tanh(x)+\tanh(y)}, \quad \operatorname{sech}(x+y) = \frac{\cosh^{-1}(x)}{\cosh(y) + x\sinh(y)}.$$

Using that $\cosh(\operatorname{arctanh}(w)) = \frac{1}{\sqrt{1-w^2}}$ and $\tanh(\operatorname{arctanh}(w)) = w$ we find

$$V(t) = \frac{1}{2}\frac{\varepsilon}{\tau N}\left(1 + \frac{\tanh\left(\frac{\varepsilon\delta t}{2}\right) + w}{1 + w\tanh\left(\frac{\varepsilon\delta t}{2}\right)}\right)u + \frac{e^{-\delta t}}{\cosh\left(\frac{\varepsilon\delta t}{2}\right) + w\sinh\left(\frac{\varepsilon\delta t}{2}\right)}V_{\ker}(t).$$

Next, we substitute back $w = \frac{2\tau}{\tau N-1}u^T V(0) - 1 = \frac{2\tau u^T V(0)}{\varepsilon} - 1$ and simplify

$$\begin{aligned}
V(t) &= \frac{1}{2}\frac{\varepsilon}{\tau N}\left(1 + \frac{\tanh\left(\frac{\varepsilon\delta t}{2}\right) + \frac{2\tau u^T V(0)}{\varepsilon} - 1}{1 + \left(\frac{2\tau u^T V(0)}{\varepsilon} - 1\right)\tanh\left(\frac{\varepsilon\delta t}{2}\right)}\right)u + \frac{e^{-\delta t}}{\cosh\left(\frac{\varepsilon\delta t}{2}\right) + \left(\frac{2\tau u^T V(0)}{\varepsilon} - 1\right)\sinh\left(\frac{\varepsilon\delta t}{2}\right)}V_{\ker}(t) \\
&= \frac{1}{2}\frac{\varepsilon}{\tau N}\frac{\left(1 + \tanh\left(\frac{\varepsilon\delta t}{2}\right)\right)\frac{2\tau u^T V(0)}{\varepsilon}}{1 + \left(\frac{2\tau u^T V(0)}{\varepsilon} - 1\right)\tanh\left(\frac{\varepsilon\delta t}{2}\right)}u + \frac{e^{-\delta t}}{\cosh\left(\frac{\varepsilon\delta t}{2}\right) + \left(\frac{2\tau u^T V(0)}{\varepsilon} - 1\right)\sinh\left(\frac{\varepsilon\delta t}{2}\right)}V_{\ker}(t) \\
&= \frac{u^T V(0)}{N}\frac{1 + \tanh\left(\frac{\varepsilon\delta t}{2}\right)}{1 + \left(\frac{2\tau u^T V(0)}{\varepsilon} - 1\right)\tanh\left(\frac{\varepsilon\delta t}{2}\right)}u + \frac{e^{-\delta t}}{\cosh\left(\frac{\varepsilon\delta t}{2}\right) + \left(\frac{2\tau u^T V(0)}{\varepsilon} - 1\right)\sinh\left(\frac{\varepsilon\delta t}{2}\right)}V_{\ker}(t).
\end{aligned}$$

Because $\lim_{\tau\to\tau_c^{(1)}} V(t) = \lim_{\varepsilon\to 0} V(t)$, we write $\tau(\varepsilon)$ as a function of ε and find

$$\lim_{\tau\to\tau_c^{(1)}} V(t) = \lim_{\varepsilon\to 0}\frac{u^T V(0)}{N}\frac{1 + \tanh\left(\frac{\varepsilon\delta t}{2}\right)}{1 + \left(\frac{2\tau(\varepsilon) u^T V(0)}{\varepsilon} - 1\right)\tanh\left(\frac{\varepsilon\delta t}{2}\right)}u + \frac{e^{-\delta t}}{\cosh\left(\frac{\varepsilon\delta t}{2}\right) + \left(\frac{2\tau(\varepsilon) u^T V(0)}{\varepsilon} - 1\right)\sinh\left(\frac{\varepsilon\delta t}{2}\right)}V_{\ker}(t),$$

which allows us to Taylor expand all functions of ε around $\varepsilon = 0$ and ignore higher order terms. The functions are $\tanh\left(\frac{\varepsilon\delta t}{2}\right) = \frac{\varepsilon\delta t}{2} + \mathcal{O}(\varepsilon^3)$, $\cosh\left(\frac{\varepsilon\delta t}{2}\right) = 1 + \mathcal{O}(\varepsilon^2)$, $\sinh\left(\frac{\varepsilon\delta t}{2}\right) = \frac{\varepsilon\delta t}{2} + \mathcal{O}(\varepsilon^3)$ and $\tau(\varepsilon) = \frac{\varepsilon+1}{N}$. After substitution and after ignoring higher order terms we find

$$\begin{aligned}
\lim_{\tau\to\tau_c^{(1)}} V(t) &= \lim_{\varepsilon\to 0}\frac{u^T V(0)}{N}\frac{1 + \frac{\varepsilon\delta t}{2}}{1 + \left(\frac{2(\varepsilon+1)u^T V(0)}{N\varepsilon} - 1\right)\frac{\varepsilon\delta t}{2}}u + \frac{e^{-\delta t}}{1 + \left(\frac{2(\varepsilon+1)u^T V(0)}{N\varepsilon} - 1\right)\frac{\varepsilon\delta t}{2}}V_{\ker}(t), \\
&= \lim_{\varepsilon\to 0}\frac{u^T V(0)}{N}\frac{1 + \frac{\varepsilon\delta t}{2}}{1 + \left(\frac{2(\varepsilon+1)u^T V(0)}{N\varepsilon} - 1\right)\frac{\varepsilon\delta t}{2}}u + \frac{e^{-\delta t}}{1 + \left(\frac{2(\varepsilon+1)u^T V(0)}{N\varepsilon} - 1\right)\frac{\varepsilon\delta t}{2}}V_{\ker}(t), \\
&= \lim_{\varepsilon\to 0}\frac{u^T V(0)}{N}\frac{1 + \frac{\varepsilon\delta t}{2}}{1 + \frac{\delta t(\varepsilon+1)u^T V(0)}{N} - \frac{\varepsilon\delta t}{2}}u + \frac{e^{-\delta t}}{1 + \frac{\delta t(\varepsilon+1)u^T V(0)}{N} - \frac{\varepsilon\delta t}{2}}V_{\ker}(t), \\
&= \frac{u^T V(0)}{N}\frac{1}{1 + \frac{\delta t u^T V(0)}{N}}u + \frac{e^{-\delta t}}{1 + \frac{\delta t u^T V(0)}{N}}V_{\ker}(t),
\end{aligned}$$

which can be rewritten as

$$V(t) = \frac{1}{\delta t + \frac{N}{u^T V(0)}} u + \frac{N e^{-\delta t}}{N + \delta t u^T V(0)} V_{\text{ker}}(t),$$

which is Eq. (7).

2. Prevalence derivation

In Eq. (16) we gave an expression for the clique prevalence without derivation. In this Appendix we show the derivation of this equation. We show that any initial condition $V_j^{(i)}(t_i)$ of the nodes in clique j yields the same prevalence expression, as long as the initial clique prevalence $y_j^{(i)}(t_i)$ stays the same.

We simplify Eq. (10) by writing

$$V_j^{(i)}(t) = W_j^{(i)}(t)u + X_j^{(i)}(t)V_{\text{ker}}^{(i)}(t_i; j) = W_j^{(i)}(t)u + X_j^{(i)}(t)\big(V_j^{(i)}(t_i) - y_j^{(i)}(t_i)u\big),$$

which follows after $V_{\text{ker}}^{(i)}(t_i; j) = (I - \frac{1}{M_j^{(i)}} uu^T)V_j^{(i)}(t_i) = V_j^{(i)}(t_i) - \frac{u^T V_j^{(i)}(t_i)}{M_j^{(i)}} u = V_j^{(i)}(t_i) - y_j^{(i)}(t_i)u$. We denote the initial infection probability of walker 1 in clique j as $v_1(t_i) = v_1$, that of walker 2 as $v_2(t_i) = v_2$ and so on. The clique prevalence $y_j^{(i)}(t)$ is now given by

$$y_j^{(i)}(t) = \frac{1}{M_j^{(i)}} \sum_{i=1}^{M_j^{(i)}} \big(W_j^{(i)}(t) + X_j^{(i)}(t)\big(v_i - y_j^{(i)}(t_i)\big)\big) = W_j^{(i)}(t) + \frac{X_j^{(i)}(t)}{M_j^{(i)}} \sum_{i=1}^{M_j^{(i)}} (v_i - y_j(t_i)). \tag{A1}$$

We can simplify the second term by substituting that the initial clique prevalence $y_j^{(i)}(t_i) = \frac{1}{M_j^{(i)}} \sum_{i=1}^{M_j^{(i)}} v_i$, which yields

$$y_j^{(i)}(t) = W_j^{(i)}(t) + \frac{X_j^{(i)}(t)}{M_j^{(i)}} \left(\sum_{i=1}^{M_j^{(i)}} v_i - \sum_{i=1}^{M_j^{(i)}} y_j^{(i)}(t_i) \right) = W_j^{(i)}(t) + \frac{X_j^{(i)}(t)}{M_j^{(i)}} \big(M_j^{(i)} y_j^{(i)}(t_i) - M_j^{(i)} y_j^{(i)}(t_i)\big) = W_j^{(i)}(t),$$

which, after substituting back the original expression of $W_j^{(i)}(t)$, and using $\frac{2\tau u^T V_j^{(i)}(t_i)}{\tau M_j^{(i)} - 1} = \frac{2y_j^{(i)}(t_i)}{1 - \frac{1}{\tau M_j^{(i)}}}$ gives Eq. (16).

3. Derivation logistic form

We rewrite the approximated clique prevalence $\hat{y}_j(t)$ in Eq. (20) to find the logistic form (21):

$$\hat{y}_j(t) = \frac{\hat{y}_{j,\infty}}{2} \left(1 + \tanh\left(\frac{\beta\theta_j - \delta}{2} t + \operatorname{arctanh}\left(2\frac{y(0)}{\hat{y}_{j,\infty}} - 1 \right) \right) \right) = \frac{\hat{y}_{j,\infty}}{2} \left(1 + \frac{\tanh\left(\frac{\beta\theta_j - \delta}{2} t\right) + 2\frac{y(0)}{\hat{y}_{j,\infty}} - 1}{1 + \tanh\left(\frac{\beta\theta_j - \delta}{2} t\right)\left(2\frac{y(0)}{\hat{y}_{j,\infty}} - 1\right)} \right),$$

where we have used that $\tanh(x + y) = \frac{\tanh(x) + \tanh(y)}{1 + \tanh(x)\tanh(y)}$. After simplification we find

$$\hat{y}_j(t) = y(0) \left(\frac{1 + \tanh\left(\frac{\beta\theta_j - \delta}{2} t\right)}{1 + \tanh\left(\frac{\beta\theta_j - \delta}{2} t\right)\left(2\frac{y(0)}{\hat{y}_{j,\infty}} - 1\right)} \right).$$

We now substitute the definition of the hyperbolic tangent $\tanh(x) = \frac{e^{2x} - 1}{e^{2x} + 1}$ to find

$$\hat{y}_j(t) = y(0) \left(\frac{\left(\frac{2e^{\gamma t}}{e^{\gamma t} + 1}\right)}{1 + \left(\frac{e^{\gamma t} - 1}{e^{\gamma t} + 1}\right)\left(2\frac{y(0)}{\hat{y}_{j,\infty}} - 1\right)} \right),$$

where we substitute $\gamma = \beta\theta_j - \delta$ for clarity. After multiplying by $\frac{e^{\gamma t} + 1}{e^{\gamma t} + 1}$ we find

$$\hat{y}_j(t) = y(0) \left(\frac{2e^{\gamma t}}{e^{\gamma t} + 1 + (e^{\gamma t} - 1)\left(2\frac{y(0)}{\hat{y}_{j,\infty}} - 1\right)} \right) = \frac{y(0) 2e^{\gamma t}}{2 + 2(e^{\gamma t} - 1)\left(\frac{y(0)}{\hat{y}_{j,\infty}}\right)}$$

$$= \frac{\hat{y}_{j,\infty}}{1 + \left(\frac{\hat{y}_{j,\infty}}{y(0)} - 1\right)e^{-\gamma t}} = \hat{y}_{j,\infty} \left(1 + \left(\frac{\hat{y}_{j,\infty}}{y(0)} - 1 \right) e^{-\gamma t} \right)^{-1} = \hat{y}_{j,\infty} \left(1 + \left(\frac{\hat{y}_{j,\infty}}{y(0)} - 1 \right) e^{-(\beta\theta_j - \delta))t} \right)^{-1}.$$

TABLE I. Summary of the baseline parameters of the NIMFA on DRWIG simulations.

Number of walkers $M = 500$	Infection rate $\beta = 0.1$
Size of walker policies $N = 25$	Curing rate $\delta = 1$
Time-step size $\Delta t = 0.5$	Policy structure = ER (N, $p = 0.5$)
Number of initially infected nodes $K = 50$	

APPENDIX B: ASSESSMENT OF THE PREVALENCE APPROXIMATION

Numerically evaluating the accuracy of our prevalence approximation (15) across the vast parameter space is unfeasible. First, we consider a baseline (Appendix B 1) for which the approximation works, then we vary the parameters one by one (Appendix B 2) to investigate their impact. Selecting for all parameters those values that perform worst, we also test a "worst case" scenario in Appendix B 3. We repeat our best and worst case tests on CRWIG in Appendix B 4.

1. Baseline

The NIMFA process on a DRWIG contact network is specified by many parameters. We will use the following baseline simulation parameters unless otherwise indicated. There are $M = 500$ walkers moving between $N = 25$ states in the Markov graph, each with a different random policy with the structure of a directed Erdős-Rényi graph with link density $p = 0.5$ and a time-step of $\Delta t = 0.5$, where the time is in units of $\frac{1}{\delta}$ as discussed in Sec. II B. We describe the generation of policies in more detail in Appendix B 2 b. The epidemic does not start until the RWIG process has had enough time to converge to the steady state. The NIMFA infection rate $\beta = 0.1$ and the curing rate $\delta = 1$. The infection rate β is chosen such that the approximated steady-state prevalence $\hat{y}_\infty = 0.5$. It follows from $0.5 = 1 - \frac{N}{\beta M} = 1 - \frac{1}{20\beta}$ that $\beta = 0.1$. The initial state has a uniformly random set of $K = 50$ walkers infected out of $M = 500$, while all others are healthy. The baseline parameters are summarized in Table I.

Figure 6 shows, on the left, the prevalence $\hat{y}(t)$ as approximated by our prevalence approximation (15). The prevalence approximation is shown in black and is compared against the NIMFA prevalence $y_{\text{NIMFA}}(t)$ on 100 DRWIG realizations, each shown with self-loops (in green) and without self-loops (in orange), simulated with the baseline parameters. In blue, the average prevalence of 100 Markovian SIS epidemics on each of the 100 DRWIG realizations is shown. Each of the 100 DRWIG realization is a Monte Carlo simulation of a fixed set of walker policies, on which the deterministic NIMFA process (with and without self-loops) and the stochastic Markovian SIS process are then simulated. The results here, and everywhere in these Appendixes, are depicted with a 50% and 100% confidence band. The light-shaded area covers 100% of simulations, while the dark-shaded area indicates the 50% of simulations closest to the mean, which is indicated with a thick line. Additionally, we include an corrected approximation (in red), where the effective infection rate τ is replaced by τ_{cor} such that the approximated steady-state prevalence equals $\hat{y}_\infty = 1 - \frac{1}{\tau d_{\text{avg}}}$ instead of $\hat{y}_\infty = 1 - \frac{1}{\tau\rho}$ as discussed in Sec. VI C. The prevalence approximation in black is hidden behind the corrected approximation in red. They overlap since $d_{\text{avg}} \approx \rho$ for the baseline parameters. On the right, the absolute error between our prevalence approximation and the simulations is shown. All figures, except those in Appendix B 2 contain the same types of data, which will not be explained again for brevity.

Interestingly, although our prevalence approximation is based on the exact solution of NIMFA with self-loops, the approximation is closer to NIMFA without self-loops. This is preferable, because self-loops are generally not considered in epidemic models. Since NIMFA is an upperbound of Markovian SIS, the prevalence without self-loops is closer to the "realistic" Markovian model as well. In Sec. VI B we observed that the approximation describes NIMFA without self-loops in the annealed regime, but NIMFA with self-loops in the quenched regime. It follows that the results in Fig. 6 suggest that for $\Delta t = 0.5$ the process is more annealed than

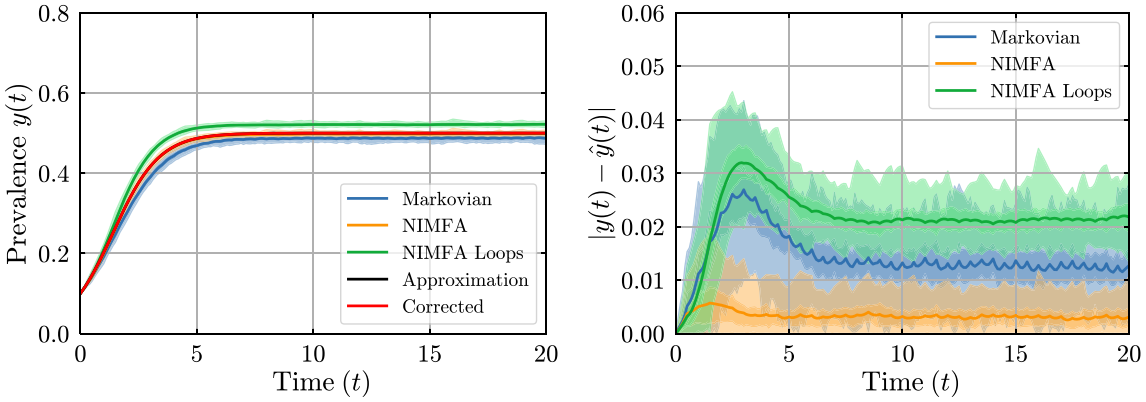


FIG. 6. Left: prevalence of Markovian SIS (blue) and NIMFA with (green) and without (orange) self-loops on discrete-time RWIG, compared with the prevalence approximation (15) and with the corrected approximation (see Sec. VI C) in black and red respectively. Right: Absolute error of our prevalence approximation (15) compared to the prevalence of Markovian SIS and NIMFA with and without self-loops on discrete-time RWIG. The baseline parameters from Table I are used.

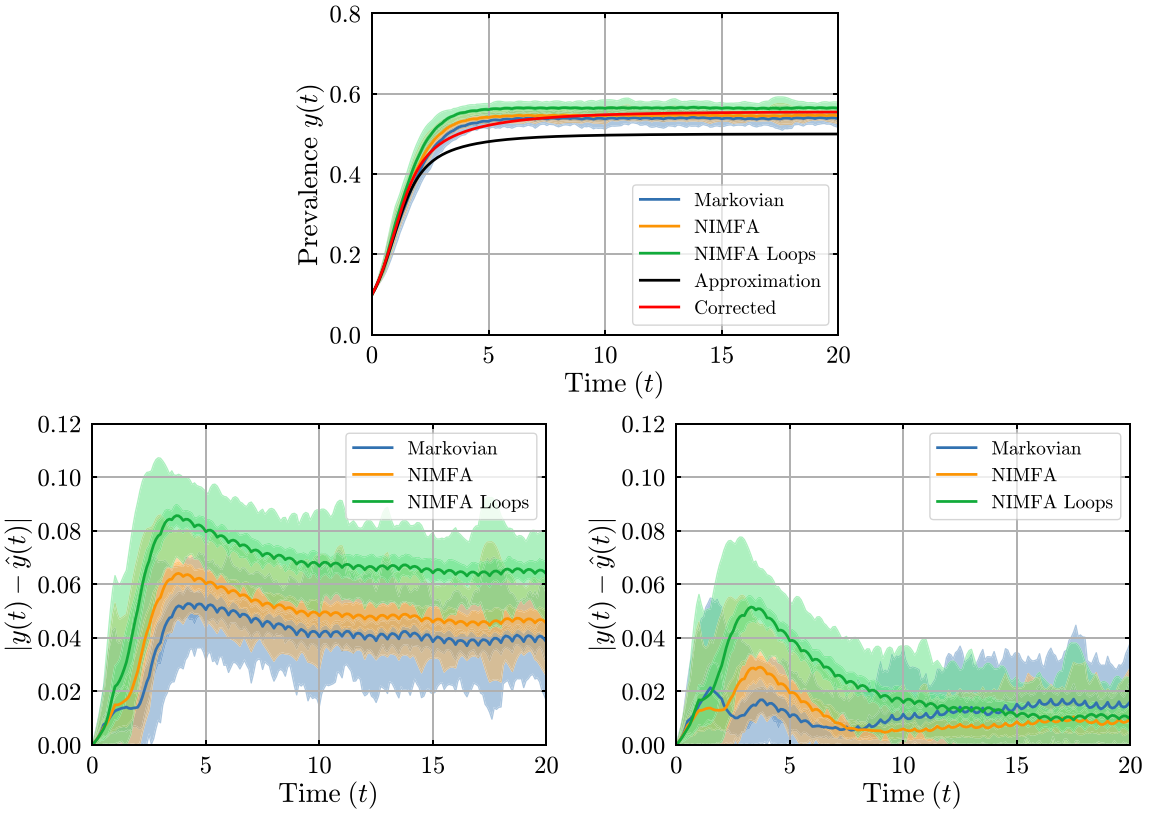


FIG. 7. Top: prevalence of Markovian SIS (blue) and NIMFA with (green) and without (orange) self-loops on discrete-time RWIG, compared with the prevalence approximation (15) and with the corrected approximation (see Sec. VI C) in black and red respectively. Bottom: Absolute error of our prevalence approximation (15) (left) and the corrected approximation (right) compared to the prevalence of Markovian SIS and NIMFA with and without self-loops on discrete-time RWIG. The baseline parameters from Table I are used, but with BA policies.

quenched. Additionally, the realization of the RWIG process has, at least with these parameters, negligible influence on the NIMFA prevalence $y(t)$. On the right, Fig. 6 shows the error made by the approximation in a baseline simulation. The highest errors occur at the start. It is likely that these high errors are an result of our approximation $V(0) \approx \hat{V}(0)$. We repeat our baseline simulation with BA policies and show the improvement gained by replacing the effective infection rate τ with the corrected effective infection rate $\tau_{\text{cor}} = \tau \frac{d_{\text{avg}}}{\rho}$. Figure 7 shows that the accuracy is improved significantly by changing the effective infection rate τ. The result for ER-policies is less interesting, because $\rho \approx d_{\text{avg}}$, which is why we did not show both accuracy plots in the ER case in Fig. 6.

We repeat these baseline simulations on CRWIG. These and the other CRWIG results are separated out into Appendix B 4 for brevity as they are very similar to the DR-WIG results, but without oscillations.

2. Variation of parameters

In this Appendix we asses the quality of Eq. (15) in Proposition 1. We show that in most cases the accuracy of our prevalence approximation (15) is still good. Specifically, we investigate:

(1) A low walker density $\rho = \frac{M}{N}$ possibly conflicts with approximations III, IV, V, and VI. We investigate the effect of the density by increasing N without increasing M.

(2) Slow contact network dynamics possibly conflict with approximations V and VI. We change the contact network dynamics by increasing the length of the discrete time-steps Δt.

(3) A RWIG steady state with, specifically a heterogeneous expected steady-state clique-size vector Θ, possibly conflicts with approximations II and III even with high walker density. We investigate this by changing the walker policies such that steady-state vectors π_m are more parallel.

(4) A heterogeneous initial infection probability vector $V(0)$ possibly conflicts with approximation VI.

(5) Starting the epidemic after shuffling the walkers randomly conflicts with approximation III, since the RWIG process is not in steady state.

a. Initial condition

We assume that the initial condition is homogeneous (i.e., the initial infection probability $v_m(0)$ is the same for every walker m) in approximation VI. Figure 8 illustrates, on the mean (left) and mean absolute error (right) of our prevalence approximation (15), as a function of the number of initially infected walkers K. Figure 8, and all other figures in this Appendix, have accuracy bands: the light-shaded area indicates 100% of the simulations, while the dark-shaded area indicates the 50% of simulations closest to the mean (thick line). All parameters are kept the same as in the base-line DRWIG NIMFA model, except for the number of initially infected

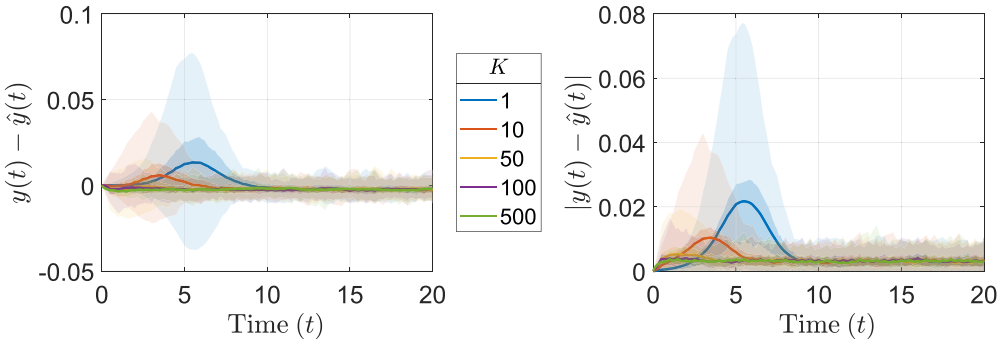


FIG. 8. Error (left) and absolute error (right) of our prevalence approximation (15) with respect to NIMFA on discrete-time RWIG without self-loops. The number of initially infected walkers K is varied.

walkers K. The largest mean errors occur when $K = 1$, which is the most extreme case investigated. However, the mean absolute error when $K = 1$ is still relatively small and less than 0.03 for the 50% band at all times t. We investigate whether the large error when $K = 1$ is due to the structure of the initial infection probability vector $V(0)$ or the small value of the initial prevalence $y(0)$. Figure 9 shows the error of our prevalence approximation (15) when the initially infected walkers are not fully infected, but have $v_m(0) = 0.1$ instead of $v_m(0) = 1$. Figure 9 indicates that lowering the initial infection probability of the K initially infected nodes increases the error of our approximation, suggesting that the initial prevalence may play a larger role in the accuracy of our approximation than the structure of the initial infection probability vector $V(0)$. The peaks in Fig. 9 have shifted in time compared to those in Fig. 8, which is most likely caused by the slower initial evolution of the epidemic.

b. Walker policies

We test if our prevalence approximation (15) fails when the walker policies have less homogeneous steady-state clique-size vectors (i.e., are made to have larger differences between steady-state clique sizes θ_j). First, we split the walkers in R groups that have the same policy. Additionally, we consider both ER-policies and BA-policies. The Erdős-Rényi (ER) policies are created from a directed ER random graph. A directed ER random graph is generated by adding each directed link $i \sim j$ to the graph with probability p. The Barabási-Albert (BA) policies are created from a BA random graph. A BA random graph is generated by starting from a clique of the first m_0 nodes and then connecting each new node randomly to m of the already existing nodes proportional to their degree. We randomly permute the labels of the nodes in the BA random graph, to avoid that the degree of a node is correlated with its label. We investigate what happens if we do not permute the nodes as well. From the random graph (ER or BA), we generate the DRWIG policy. First, we add with probability $\frac{1}{2}$ a self-loop to each node in the adjacency matrix A. Then we divide each row i of the adjacency matrix A by the degree d_i of node i, such that we have a transition probability matrix P, which will be the walker policy. Because the policy size is $N = 25$, the BA graphs do not have their characteristic power-law degree distribution. This is not a problem for us, because we are only interested in creating a hub-structure to increase the variance of steady-state clique-size vector Θ. We found that the steady-state clique-size vector Θ has a larger variance between its elements when the policies are nonpermuted BA policies. The variance between the elements of the steady-state clique-size vector Θ is small for ER policies and permuted BA policies.

Figures 10 and 11 show for both ER policies and BA policies the error of our prevalence approximation (15), for different numbers of walker policies R. For both ER and BA policies, the largest error is when there is a single policy for all walkers ($R = 1$), but the errors for BA policies are much larger than for ER policies.

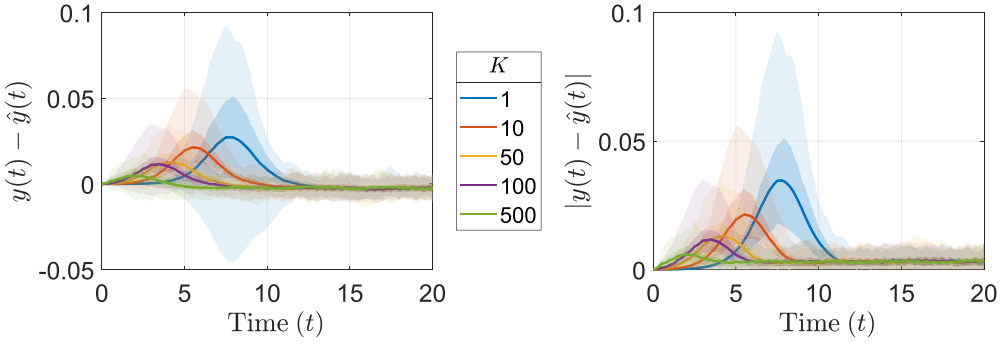


FIG. 9. Error (left) and absolute error (right) of our prevalence approximation (15) with respect to NIMFA on discrete-time RWIG without self-loops. The number of initially infected walkers K is varied. Additionally, the initially infected walkers have $v_m(0) = 0.1$ instead of $v_m(0) = 1$.

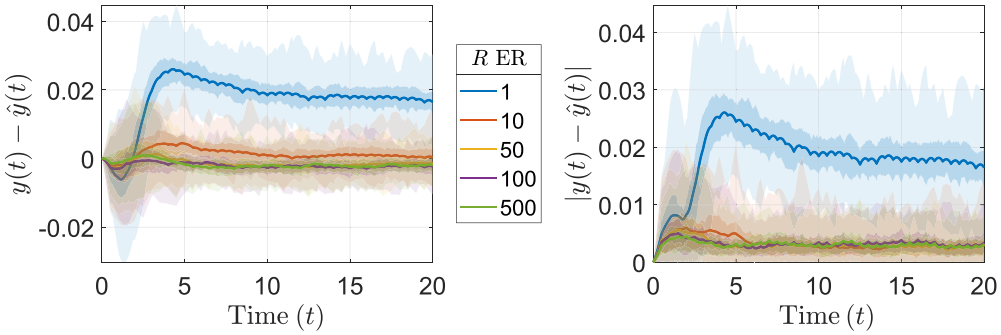


FIG. 10. Error (left) and absolute error (right) of our prevalence approximation (15) with respect to NIMFA on discrete-time RWIG without self-loops. The number of different walker policies R is varied.

Next, we increase the size of the walker policy N to lower the walker density $\rho = \frac{M}{N}$. In these simulations, the infection rate β is fixed as $\beta = \frac{N}{250}$, such that the approximated steady-state prevalence $\hat{y}_\infty$ is constant. If we do not change β as well as N, the epidemic will go below the threshold, because the same amount of walkers ($M = 500$) are distributed over a larger number of locations, resulting in smaller cliques with lower thresholds. If the infection rate $\beta = \tau$ does not grow with N, the effective infection rate τ will eventually be smaller than the lowering thresholds and the results will no longer be qualitatively comparable. Figures 12 and 13 show the error of our prevalence approximation (15) as a function of the policy size N for ER and BA policies respectively. The green lines in Figs. 12 and 13, corresponding to $N = 500$, clearly show oscillations. These oscillations can, to a lesser extend, also be observed in Figs. 10 and 11. The oscillations are caused by the changes in the temporal contact graph: after each contact graph change the epidemic process has to converge to the new steady state. Interestingly, the amplitude of the oscillations in Figs. 12 and 13 grows with N. We hypothesize that the increase of the oscillation amplitudes when N increases is due to the low walker density $\rho = 1$. We argued, in approximation III, that the fluctuations of the clique sizes in an RWIG process around the steady-state clique size vector Θ would be small if the number of walkers M is big enough by invoking Kolmogorov's law. At low walker densities ρ, the epidemic may be sensitive to these small fluctuations, because the increase of the steady-state prevalence when the size of a clique increases by a fixed amount, decreases significantly for larger clique sizes θ. The derivative $\frac{dy_\infty}{d\theta} = \frac{1}{\tau\theta^2}$ of the steady-state prevalence $y_\infty = 1 - \frac{1}{\tau\theta}$, indicates that adding or removing a single walker to a small clique (say $\theta < 4$) has significantly more impact on the steady-state prevalence than adding or removing a single walker to a larger clique (say $\theta > 20$). Therefore, at low walker densities ρ (and thus low steady-state clique sizes θ_j), the impact of the fluctuations of the actual number of walkers in a location j around the steady-state clique size θ_j have more impact on the epidemic.

We repeated the two experiments above with a modified BA policy: instead or randomly permuting the nodes, we kept the original labels of the BA graph for all walkers. This means that the order in which each node is added was the same for each walker resulting in a more heterogeneous steady-state clique-size vector Θ. The results are shown in Figs. 14 and 15, with the number of different walker policies R varied in Fig. 14 and the number of locations N varied in Fig. 15. The errors of the unpermuted BA policies are larger than those in of the permuted BA policies. The oscillations of the green and purple lines in the right panel of Fig. 15 are also larger than those in Fig. 13. We hypothesize that the steady-state clique-size vector Θ has more large elements due to the labeling of the BA policy and therefore, because the elements sum to M, also even more small elements, which, as we explained above, could be a factor determining the magnitude of the oscillations. Because all walkers already share the same hub nodes due to the underlying BA graphs, changing the number of policies R has little effect on the epidemic, as visible by the overlapping lines in Fig. 14. An interesting observation

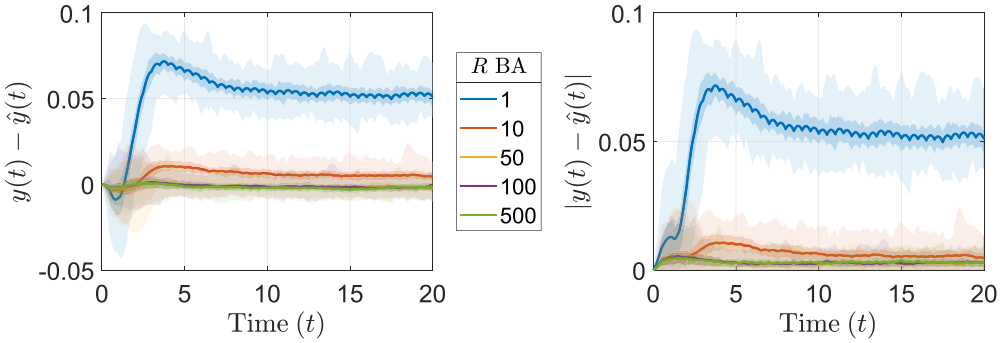


FIG. 11. Error (left) and absolute error (right) of our prevalence approximation (15) with respect to NIMFA on discrete-time RWIG without self-loops. The number of different walker policies R is varied. Additionally, the walkers have BA policies.

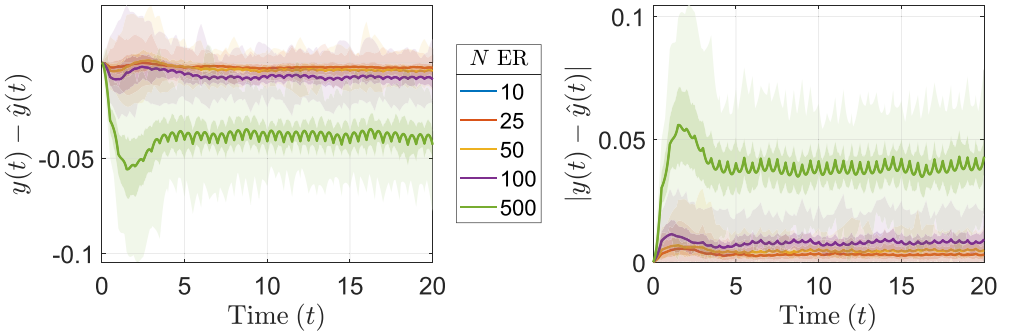


FIG. 12. Error (left) and absolute error (right) of our prevalence approximation (15) with respect to NIMFA on discrete-time RWIG without self-loops. The policy size N is varied.

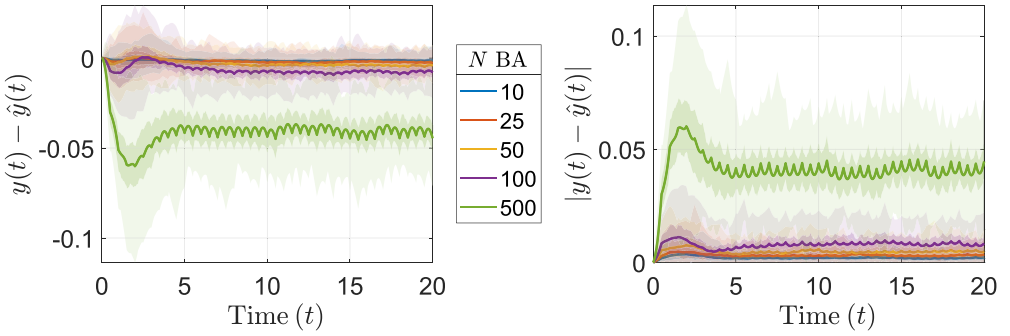


FIG. 13. Error (left) and absolute error (right) of our prevalence approximation (15) with respect to NIMFA on discrete-time RWIG without self-loops. The policy size N is varied. Additionally, the walkers have BA policies.

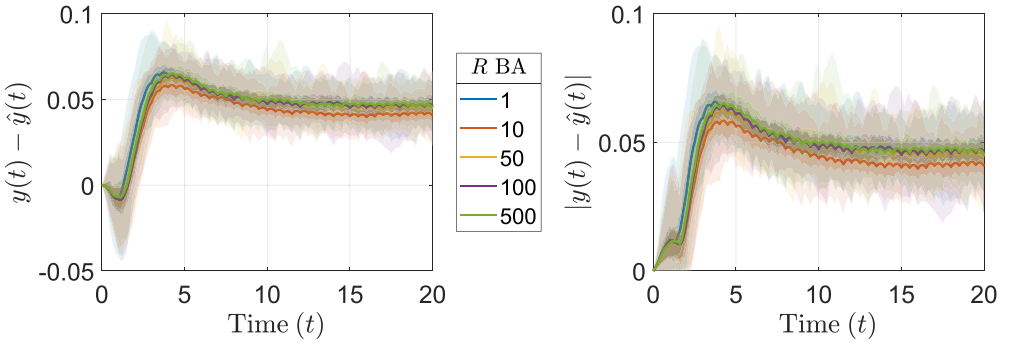


FIG. 14. Error (left) and absolute error (right) of our prevalence approximation (15) with respect to NIMFA on discrete-time RWIG without self-loops. The number of different walker policies R is varied. Additionally, the walkers have BA-policies with the same node ordering.

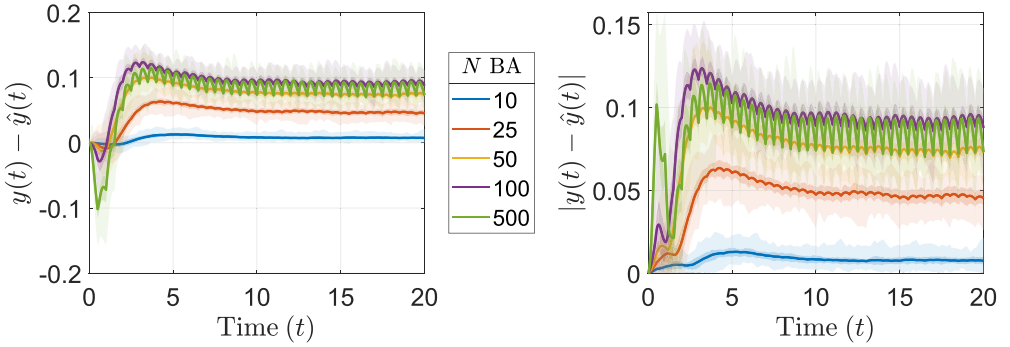


FIG. 15. Error (left) and absolute error (right) of our prevalence approximation (15) with respect to NIMFA on discrete-time RWIG without self-loops. The policy size N is varied. Additionally, the walkers have BA-policies with the same node ordering.

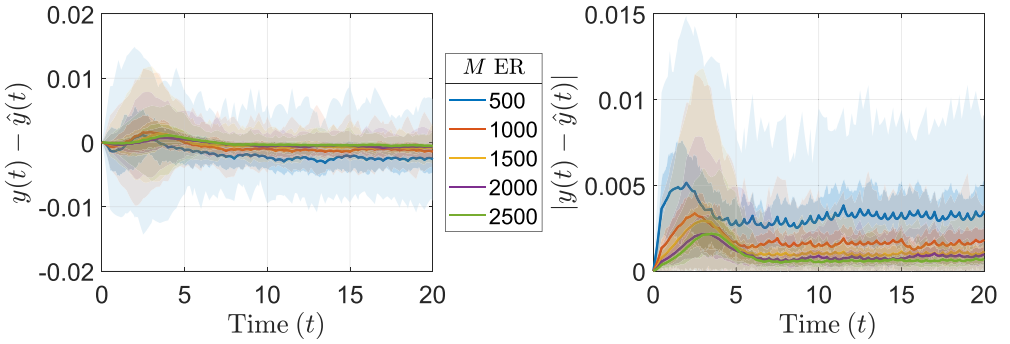


FIG. 16. Error (left) and absolute error (right) of our prevalence approximation (15) with respect to NIMFA on discrete-time RWIG without self-loops. The number of walkers M is varied.

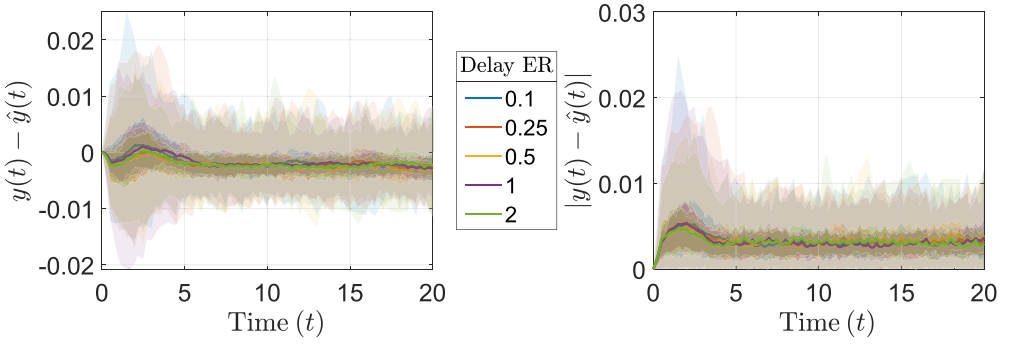


FIG. 17. Error (left) and absolute error (right) of our prevalence approximation (15) with respect to NIMFA on discrete-time RWIG without self-loops. The delay between the start of the RWIG and NIMFA process is varied.

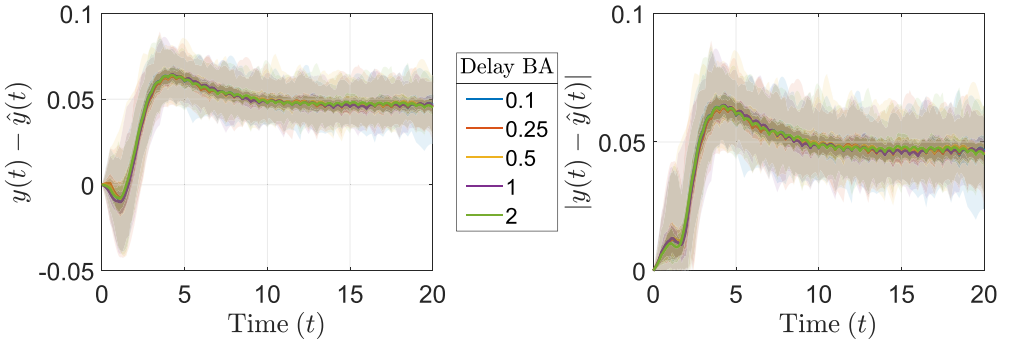


FIG. 18. Error (left) and absolute error (right) of our prevalence approximation (15) with respect to NIMFA on discrete-time RWIG without self-loops. The delay between the start of the RWIG and NIMFA process is varied. Additionally, the walkers have BA-policies.

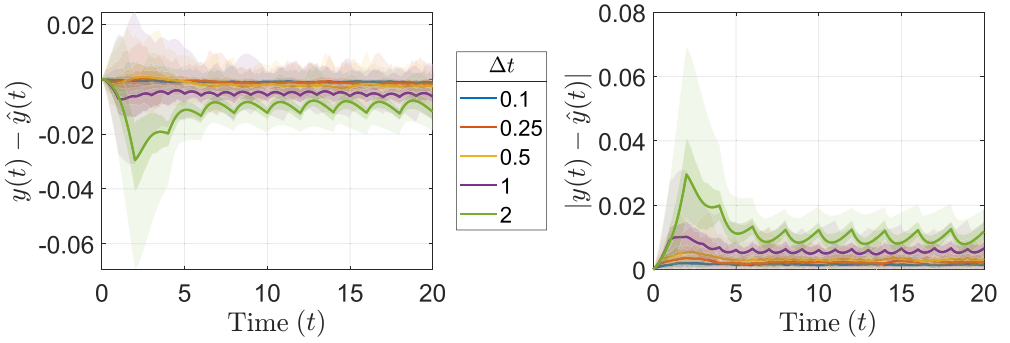


FIG. 19. Error (left) and absolute error (right) of our prevalence approximation (15) with respect to NIMFA on discrete-time RWIG without self-loops. The time-step size Δt of DRWIG is varied.

TABLE II. Summary of the parameters of our "worst case" NIMFA on DRWIG simulations.

Number of walkers $M = 500$	Infection rate $\beta = 2$
Size of walker policies $N = 500$	Curing rate $\delta = 1$
Time-step size $\Delta t = 0.5$	Policy structure = BA $(N, 5, 5)$ and same node order
Number of initially infected nodes $K = 1$	

in Fig. 15 is that the approximation is more accurate for $N = 500$ than $N = 100$. It is unclear what exactly causes this improvement, but the improvement could be related to the fact that BA graphs only start showing their scale-free properties from sizes around $N = 500$, with the true scale-free structures only appearing for significantly larger graphs.

Last, we vary the number of walker M in Fig. 16. As with the policy size N, we varied β together with M such that the approximated steady state was always $\hat{y}_\infty = 0.5$. We observe that the prevalence approximation becomes more accurate the larger M becomes. We think the prevalence performs good for large walker density ρ because, as discussed above, the larger θ_j, the less impact variation in θ_j has on the prevalence.

c. *RWIG speed and convergence*

We assume in approximation III that the DRWIG process is in the steady state. In our baseline model we allow the RWIG process to reach the steady state before starting the epidemic. We now investigate what happens if the RWIG process has not converged yet at the start of the epidemic. In other words: we investigate what happens when the epidemic starts during the "warm-up period" of the RWIG process, instead of after convergence. In the baseline simulation the epidemic is started after 100 DRWIG time-steps, which is far sufficient for convergence to the steady state because the process converges exponentially fast [8]. We call the time between the start of the RWIG process and the start of the epidemic process the *epidemic delay*. In Fig. 17, the error of the baseline process with different epidemic delays is shown. The results shown suggest that the epidemic delay does not impact the error. The curves are all comparable to the average of the baseline in the right panel of Fig. 6. Because the steady-state distribution of the walkers with ER policies is quite uniform and DRWIG is initiated uniformly at random, we also considered walkers with unpermuted BA policies. Their steady state is less uniform, but Fig. 18 indicates that the delay has no impact on the error in the BA case either. We also varied the time-step size Δt of the DRWIG process. In Fig. 19, the error of our prevalence approximation is shown for different values of

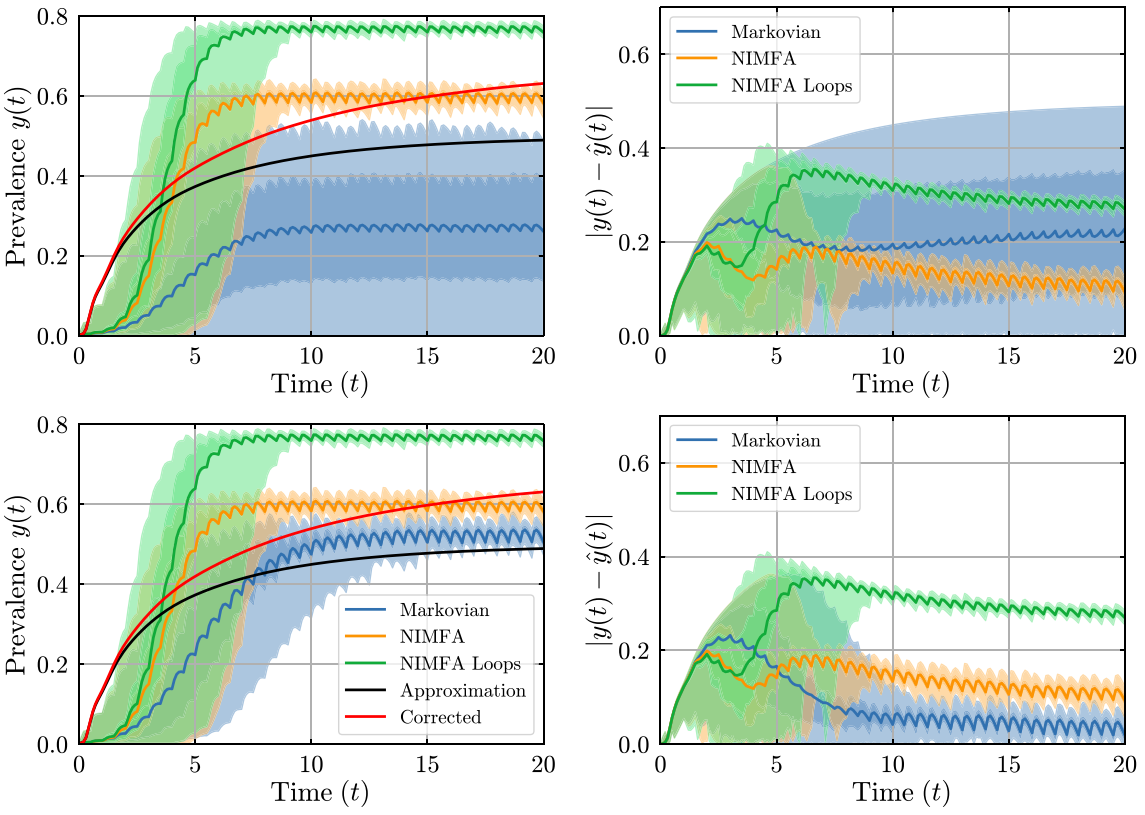


FIG. 20. Left: prevalence of Markovian SIS (blue; top: with die-outs, bottom: no die-outs) and NIMFA with (green) and without (orange) self-loops on discrete-time RWIG, compared with the prevalence approximation (15) and with the corrected approximation (see Sec. VI C) in black and red respectively. Right: Absolute error of our prevalence approximation (15) compared to the prevalence of Markovian SIS and NIMFA with and without self-loops on discrete-time RWIG. The "worst case" parameters from Table II are used.

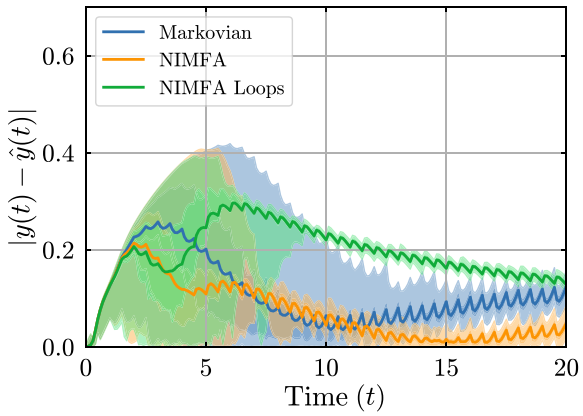


FIG. 21. Absolute error of the corrected approximation compared to the prevalence of Markovian SIS (no die-outs) and NIMFA with and without self-loops on discrete-time RWIG. The "worst case" parameters from Table II are used.

the time-step Δt. The large error for small times for $\Delta t = 2$ can likely be explained by the disease not spreading to all locations in one DRWIG transition. We observe that the error decreases if Δt decreases. Additionally, we observe that the error in the steady state increases with Δt, both observations in agreement with our findings in Sec. VI.

3. Worst case

In Appendix B 2, we varied individual parameters from the baseline. Now, we select, for each parameter, the value with the highest mean absolute error, which we will interpret as a worst case scenario. There are two exceptions. First, the time-step size Δt is kept at its baseline value of $\Delta t = 0.5$ and not the worst performing value $\Delta t = 2$ in Fig. 19, for timescale consistency. Second, we did not reduce the initial infection probability of patient zero to $v_m(0) = 0.1$, like on the right in Fig. 8, because we wanted to have an initial condition that is valid in Markovian SIS as well. Table II shows the parameters used.

Figure 20 shows the simulation results of the our "worst case" scenario. Figure 20 considers two different Markovian processes: on the top, Fig. 20 shows NIMFA (with and without self-loops) and a regular Markovian SIS process, while on the bottom, Fig. 20 shows the same NIMFA (with and without self-loops) and Markovian SIS conditioned on no die-outs. Specifically, in this conditional process, any time there is a single infected walker and they cure, they are immediately reinfected. The effect of die-outs in a low walker density simulation with only a single initially infected walker is significant. The effect of die-outs was not significant under the baseline parameters and is therefore not considered in Fig. 6 or Fig. 7. Because the Markovian Monte Carlo SIS epidemics in Fig. 20 are all simulated on the same DRWIG realizations, we can directly compare the top left panel with the bottom left panel. Any difference in the Markovian prevalence $y_{\mathrm{SIS}}(t)$ between the top left and bottom left panels is due to (early) die-outs.

Our approximation underestimates the prevalence significantly and also reaches the steady state slower. Possibly, our steady-state clique size vector Θ underestimates the probability of a group of walkers being in the same space. Since the walker density $\rho = 1$, if all walkers are spread evenly one would expect one walker in each location. However, in the DRWIG NIMFA epidemic, cliques larger than one are most likely very common: if the M walkers are distributed uniformly over the N locations, the probability a walker is alone in its location is approximately $(\frac{N-1}{N})^{(M-1)} \approx 0.37$, when $N = M = 500$.

Because NIMFA does not consider die-outs [26] and models the metastable state of Markovian SIS above the epidemic threshold $\tau_c^{(1)}$, our approximation, like NIMFA, should be compared with the no die-out Markovian process above the threshold. Because NIMFA upperbounds the Markovian SIS process, the underestimation of the NIMFA steady-state prevalence by our approximation (15) is of a lesser magnitude for the Markovian SIS prevalence when using the "worst case" parameters.

Additionally, the shape of the error curve in Fig. 20 is very similar to the error curve for $N = 500$ on the right of Fig. 14 in Appendix B 2, implying that the error in the worst case is

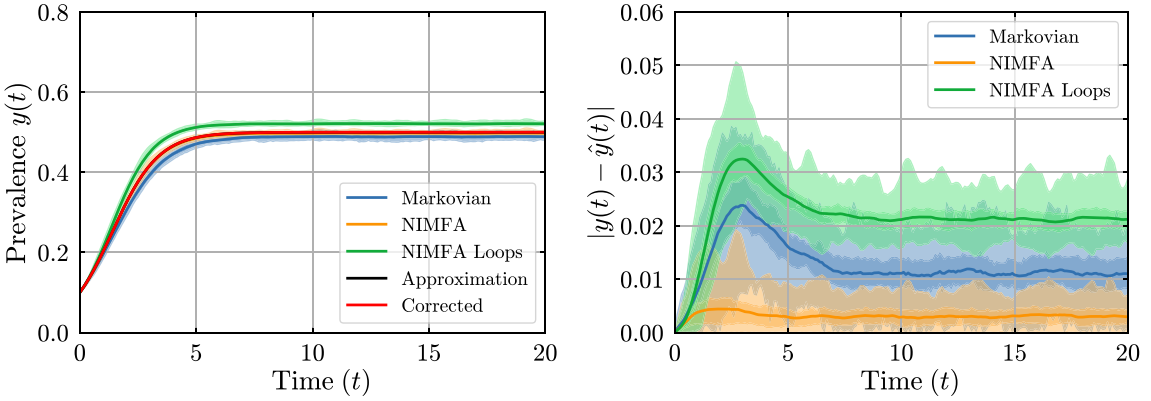


FIG. 22. Left: prevalence of Markovian SIS (blue) and NIMFA with (green) and without (orange) self-loops on continuous-time RWIG, compared with the prevalence approximation (15) and with the corrected approximation (see Sec. VI C) in black and red respectively. Right: Absolute error of our prevalence approximation (15) compared to the prevalence of Markovian SIS and NIMFA with and without self-loops on continuous-time RWIG. The baseline parameters from Table I are used.

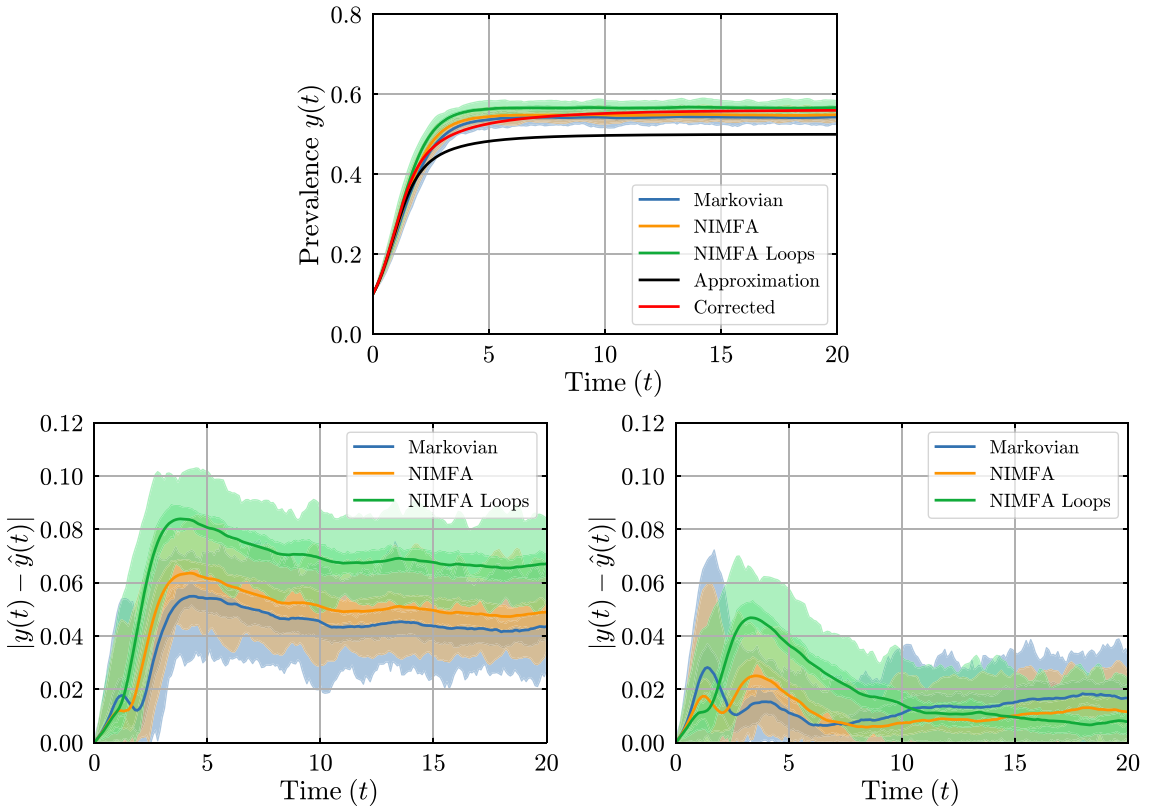


FIG. 23. Top: prevalence of Markovian SIS (blue) and NIMFA with (green) and without (orange) self-loops on continuous-time RWIG, compared with the prevalence approximation (15) and with the corrected approximation (see Sec. VI C) in black and red respectively. Bottom: Absolute error of our prevalence approximation (15) (left) and the corrected approximation (right) compared to the prevalence of Markovian SIS and NIMFA with and without self-loops on continuous-time RWIG. The baseline parameters from Table I are used, but with BA policies.

dominated by the policy size. It is plausible that the weakness of approximation III at low walker densities ρ and on labeled BA policies (see also Figs. 12 and 14) is the largest cause of the errors in the "worst case" shown in Fig. 20. Comparing the bottom right of Fig. 20 with Fig. 21, shows that the corrected approximation has an improved accuracy.

4. Prevalence approximation on CRWIG

We repeat all baseline and worst case simulations on CRWIG. The DRWIG time-step Δt is used as the expected sojourn time in CRWIG, such that the mobility of individual walkers in both models is comparable. The left of Fig. 22 shows the prevalence under the baseline parameters (Table I). The simulations on the baseline with BA-policies is shown in Fig. 23. The results for the "worst case" parameters (Table II) in CRWIG are shown in Fig. 24. The error of the corrected approximation for the worst case on CRWIG is shown in Fig. 25. All CRWIG results are very similar to their DRWIG equivalents. The main difference being that the curves are smoother because walker movements are less bursty.

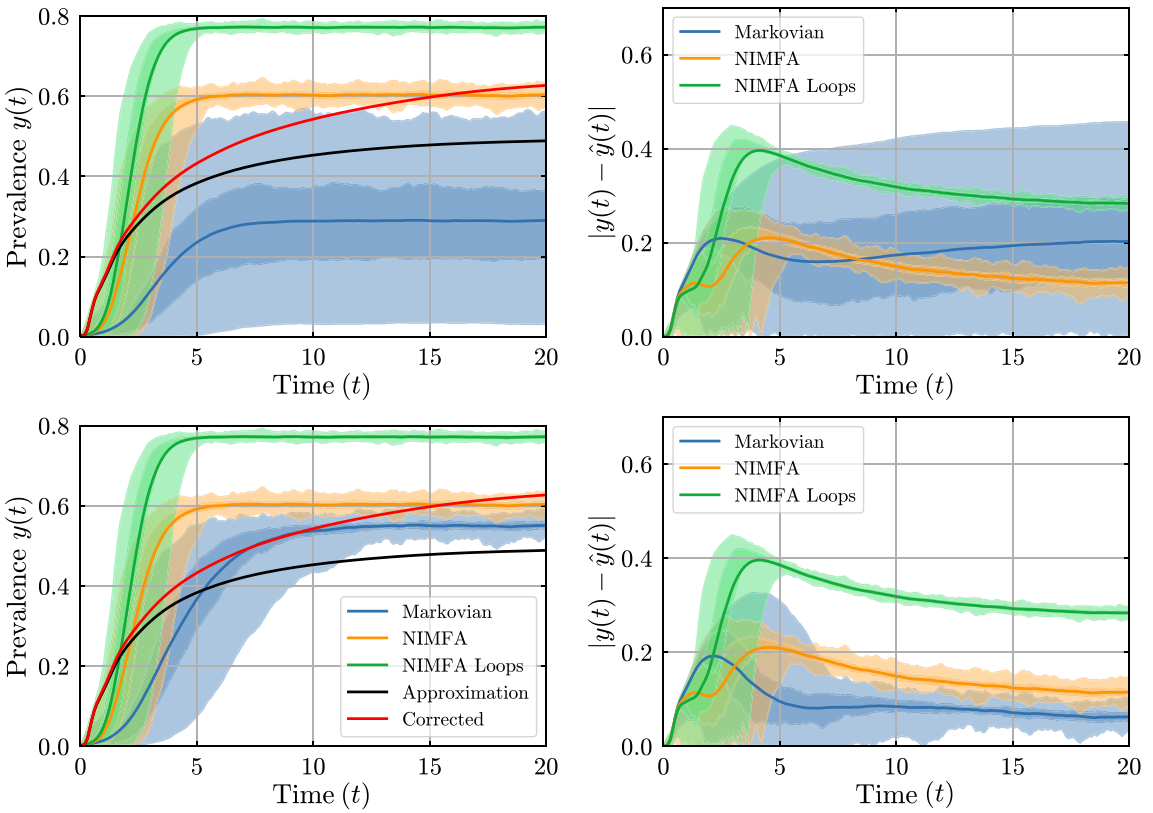


FIG. 24. Left: prevalence of Markovian SIS (blue; top: with die-outs, bottom: no die-outs) and NIMFA with (green) and without (orange) self-loops on continuous-time RWIG, compared with the prevalence approximation (15) and with the corrected approximation (see Sec. VI C) in black and red respectively. Right: Absolute error of our prevalence approximation (15) compared to the prevalence of Markovian SIS and NIMFA with and without self-loops on continuous-time RWIG. The "worst case" parameters from Table II are used.

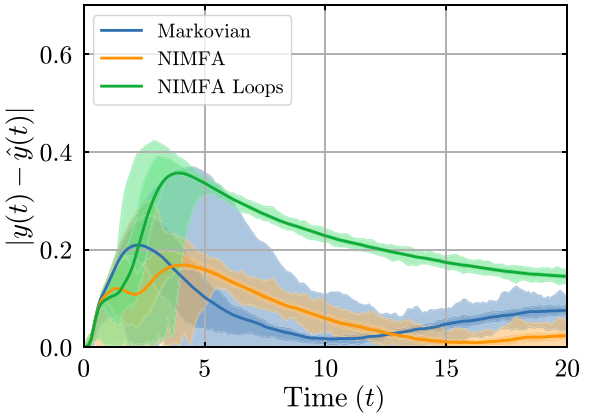


FIG. 25. Absolute error of the corrected approximation compared to the prevalence of Markovian SIS (no die-outs) and NIMFA with and without self-loops on continuous-time RWIG. The "worst case" parameters from Table II are used.

[1] N. Masuda and R. Lambiotte, *A Guide to Temporal Networks* (World Scientific, Singapore, 2016).
[2] V. Colizza and A. Vespignani, Epidemic modeling in metapopulation systems with heterogeneous coupling pattern: Theory and simulations, J. Theor. Biol. **251**, 450 (2008).
[3] D. Balcan, V. Colizza, B. Gonçalves, H. Hu, J. J. Ramasco, and A. Vespignani, Multiscale mobility networks and the spatial spreading of infectious diseases, Proc. Natl. Acad. Sci. USA **106**, 21484 (2009).
[4] D. Colombi, C. Poletto, E. Nakouné, H. Bourhy, and V. Colizza, Long-range movements coupled with heterogeneous incubation period sustain dog rabies at the national scale in Africa, PLoS Neglected Trop. Dis. **14**, e0008317 (2020).
[5] M. Chinazzi, J. T. Davis, M. Ajelli, C. Gioannini, M. Litvinova, S. Merler, A. Pastore y Piontti, K. Mu, L. Rossi, K. Sun, C. Viboud, X. Xiong, H. Yu, M. E. Halloran, I. M. Longini, Jr., and A. Vespignani, The effect of travel restrictions on the spread of the 2019 novel coronavirus (COVID-19) outbreak, Science **368**, 395 (2020).
[6] W. O. Kermack and A. G. McKendrick, A contribution to the mathematical theory of epidemics, Proc. R. Soc. London, Ser. A **115**, 700 (1927).
[7] A.-D. Almasan, S. Shvydun, I. Scholtes, and P. Van Mieghem, Generating temporal contact graphs using random walkers, IEEE Trans. Network Sci. Eng. **12**, 1649 (2025).
[8] R. Persoons, M. D'Alessandro, and P. Van Mieghem, Continuous-time process for human contact dynamics, Phys. Rev. E **112**, 034310 (2025).
[9] M. Génois and A. Barrat, Can co-location be used as a proxy for face-to-face contacts? EPJ Data Sci. **7**, 11 (2018).
[10] B. A. Prakash, H. Tong, N. Valler, M. Faloutsos, and C. Faloutsos, in *Proceedings of the European Conference on Machine Learning and Knowledge Discovery in Databases (ECML PKDD'10), Barcelona, Spain, Part III 21* (Springer, Berlin, 2010), pp. 99–114.
[11] E. Valdano, L. Ferreri, C. Poletto, and V. Colizza, Analytical computation of the epidemic threshold on temporal networks, Phys. Rev. X **5**, 021005 (2015).
[12] E. Valdano, M. R. Fiorentin, C. Poletto, and V. Colizza, Epidemic threshold in continuous-time evolving networks, Phys. Rev. Lett. **120**, 068302 (2018).
[13] N. Perra, B. Gonçalves, R. Pastor-Satorras, and A. Vespignani, Activity driven modeling of time varying networks, Sci. Rep. **2**, 469 (2012).
[14] G. St-Onge, J.-G. Young, E. Laurence, C. Murphy, and L. J. Dubé, Phase transition of the susceptible-infected-susceptible dynamics on time-varying configuration model networks, Phys. Rev. E **97**, 022305 (2018).
[15] A. Koher, H. H. Lentz, J. P. Gleeson, and P. Hövel, Contact-based model for epidemic spreading on temporal networks, Phys. Rev. X **9**, 031017 (2019).
[16] Y.-Q. Zhang, X. Li, and A. V. Vasilakos, Spectral analysis of epidemic thresholds of temporal networks, IEEE Trans. Cybern. **50**, 1965 (2017).
[17] V. Kohar and S. Sinha, Emergence of epidemics in rapidly varying networks, Chaos, Solitons Fractals **54**, 127 (2013).
[18] B. Prasse, K. Devriendt, and P. Van Mieghem, Clustering for epidemics on networks: A geometric approach, Chaos **31**, 063115 (2021).
[19] R. Persoons, M. Sensi, B. Prasse, and P. Van Mieghem, Transition from time-variant to static networks: Timescale separation in N-intertwined mean-field approximation of susceptible-infectious-susceptible epidemics, Phys. Rev. E **109**, 034308 (2024).
[20] P. Van Mieghem, J. Omic, and R. Kooij, Virus spread in networks, IEEE/ACM Trans. Netw. **17**, 1 (2008).
[21] P. Van Mieghem, The N-intertwined SIS epidemic network model, Computing **93**, 147 (2011).
[22] P. Van Mieghem, *Performance Analysis of Complex Networks and Systems* (Cambridge University Press, Cambridge, UK, 2014).
[23] R. Pastor-Satorras, C. Castellano, P. Van Mieghem, and A. Vespignani, Epidemic processes in complex networks, Rev. Mod. Phys. **87**, 925 (2015).
[24] D. Bichara, Y. Kang, C. Castillo-Chavez, R. Horan, and C. Perrings, SIS and SIR epidemic models under virtual dispersal, Bull. Math. Biol. **77**, 2004 (2015).
[25] A. N. Kolmogorov, Sulla determinazione empirica di una legge di distribuzione, Giorn. Dell'Inst. Ital. Degli Att. **4**, 89 (1933).
[26] Q. Liu and P. Van Mieghem, in *Proceedings of the International Workshop on Complex Networks and Their Applications* (Springer, Berlin, 2016), pp. 511–521.